

## Distribution of alkylamines in surface waters around the Antarctic Peninsula and Weddell Sea

Arianna Rocchi<sup>1,2</sup>, Mark F. Fitzsimons<sup>3</sup>, Preston Akenga<sup>3</sup>, Ana Sotomayor<sup>4</sup>, Elisabet L. Sà<sup>1</sup>, Queralt Güell-Bujons<sup>1</sup>, Magda Vila<sup>1</sup>, Yaiza M. Castillo<sup>1</sup>, Manuel Dall'Osto<sup>1</sup>, Dolors Vaqué<sup>1</sup>, Charel Wohl<sup>1,5,6</sup>, Rafel Simó<sup>1</sup> and Elisa Berdalet<sup>1</sup>

<sup>1</sup>Department of Marine Biology and Oceanography, Institute of Marine Sciences (ICM), CSIC, Barcelona, E-08003, Spain.

<sup>2</sup>Faculty of Earth Sciences, University of Barcelona, Barcelona, E-08028, Spain.

<sup>3</sup>Biogeochemistry Research Centre, School of Geography, Earth and Environmental Sciences, University of Plymouth, Plymouth, PL4 8AA, UK.

<sup>4</sup>Marine Technology Unit (UTM), CSIC, Pg Marítim de la Barceloneta, 37-49, Barcelona, E-08003, Spain.

<sup>5</sup>Centre of Ocean and Atmospheric Sciences, School of Environmental Sciences, University of East Anglia, Norwich, NR4 7TJ, UK.

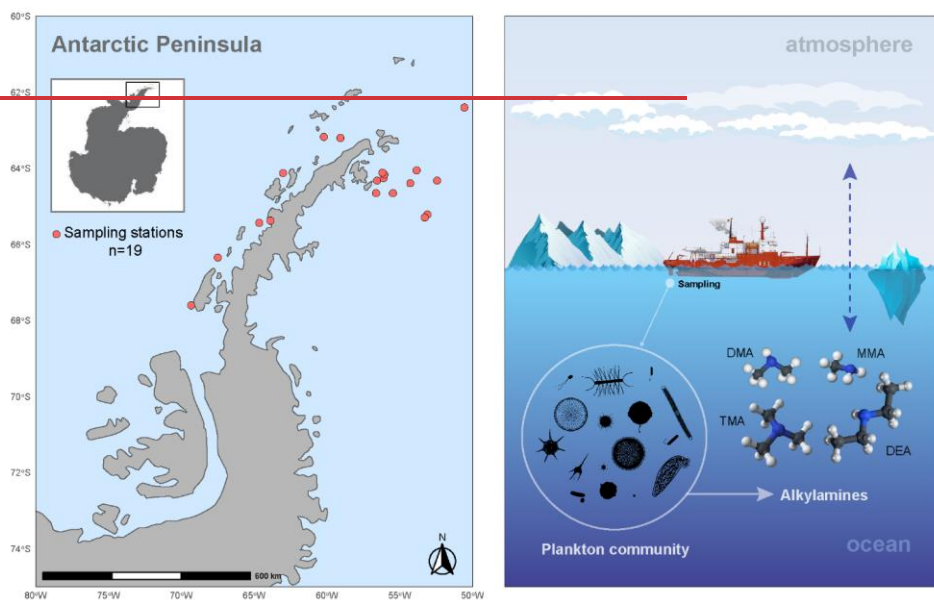
<sup>6</sup>National Centre for Atmospheric Science, University of East Anglia, Norwich, NR4 7TJ, UK.

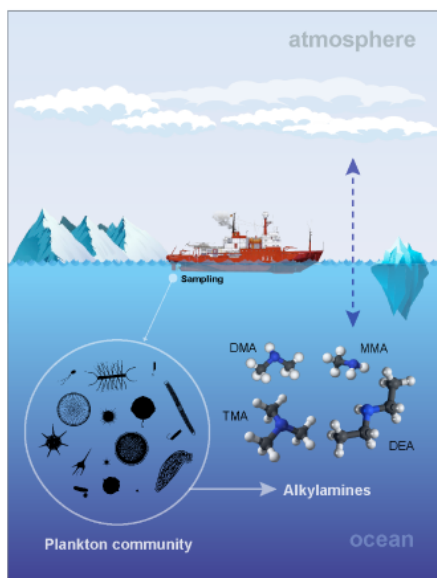
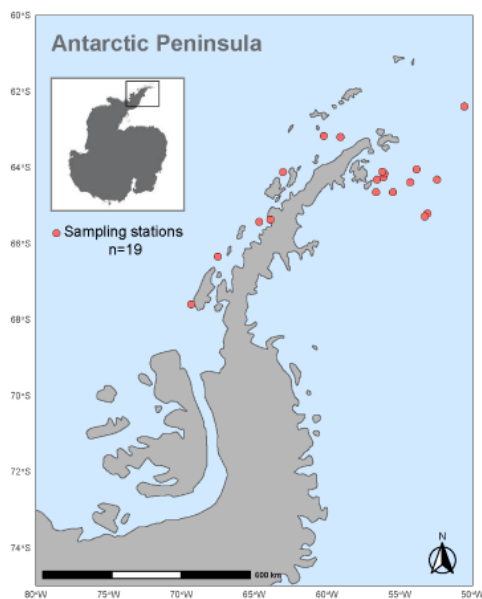
Correspondence to: Arianna Rocchi ([rocchi@icm.csic.es](mailto:rocchi@icm.csic.es)), Elisa Berdalet ([berdalet@icm.csic.es](mailto:berdalet@icm.csic.es))

**Abstract.** ~~Small molecular weight alkylamines~~, Alkylamines, volatile organic nitrogen compounds with small molecular weight, are present in the surface ocean, participate in the marine biogeochemical nitrogen cycle, atmospheric ~~processes~~ chemistry and cloud formation. Alkylamines have been detected in polar regions, suggesting that these areas constitute emission hotspots of these compounds. However, knowledge of the sea surface distribution patterns and factors ~~controlling/modulating~~ alkylamines ~~remains~~ remain limited due to their high reactivity and low concentrations, which hamper accurate measurements. We investigated the presence and distribution of alkylamines in ~~waters~~ seawaters around the Antarctic Peninsula and the northern Weddell Sea during the late austral summer and explored their potential links to marine microbiota. Alkylamines were ubiquitous in all analyzed samples ~~measured~~, accounting for ~2 % of the dissolved and particulate organic nitrogen pool. The ~~unique~~ only particulate form found was trimethylamine (TMA), detected for the first time in Antarctic waters ~~accounting for at~~ concentrations of  $9.7 \pm 4.6$  nM. We efficiently measured dissolved trimethylamine (TMA,  $20.9 \pm 15.2$  nM), dimethylamine (DMA,  $32.3 \pm 32.7$  nM) and diethylamine (DEA,  $7.2 \pm 1.7$  nM) across the surveyed area, while dissolved monomethylamine (MMA,  $12.7 \pm 0.1$  nM) remained below detection limit in most samples. ~~Our findings reveal spatial variations~~ Variations in alkylamine concentrations ~~that~~ did not align with the overall phytoplankton biomass but with specific biological components. TMA was predominantly associated with, and released from,

ha formattato: Colore carattere: Rosso

nanophytoplankton. DMA was likely produced by the degradation of TMA or trimethylamine oxide by nanophytoplankton cells or associated [heterotrophic](#) bacteria. The sources of DEA remain unclear but were suggestive of a distinct biogeochemical pathway from those of TMA and DMA. MMA is thought to primarily originate from bacterial degradation of nitrogen-based osmolytes or amino acids, but detection in too few samples precluded any robust association with microbiota. This study reveals that volatile alkylamines are widespread in Antarctic surface waters, where they are primarily sourced from nanophytoplankton cells and associated heterotrophic bacteria and protists.





**Short summary.** During the ~~Polar-Change~~PolarChange expedition, volatile alkylamines, important players in nitrogen cycling and cloud formation, were measured in Antarctic waters using a high-sensitivity method. Trimethylamine was the dominant alkylamine in marine particles, associated with nanophytoplankton. Dissolved dimethylamine likely originated from trimethylamine degradation, while diethylamine sources remain unclear. These findings confirm the biological origin of alkylamines in polar marine microbial food webs.

ha formattato: Tipo di carattere: Grassetto

## 1 Introduction

The marine organic nitrogen (ON) pool is an important natural reservoir of reactive molecules, containing biologically relevant compounds which contribute to biogeochemical cycles in the surface ocean and ocean-atmosphere-climate interactions. Among them, alkylamines are low-molecular weight (<100 Da) polar molecules that exhibit high solubility in seawater and high vapor pressure. Alkylamines are emitted from the ocean to the atmosphere 1) via sea spray, contributing

to a highly variable nitrogen-containing fraction of primary aerosol (Dall'Osto et al., 2017; Liu et al., 2022) aerosols (Dall'Osto et al., 2017; Liu et al., 2022), and 2) through gas exchange, where they are efficiently incorporated into secondary marine aerosols and contribute to very fast new particle formation events (Brean et al., 2021; Corral et al., 2022; Ning et al., 2022; Zu et al., 2024). (Brean et al., 2021; Corral et al., 2022; Ning et al., 2022; Zu et al., 2024). Additionally, Antarctic sea-ice microbiota and sea-ice-influenced ocean systems are significant sources of dissolved organic nitrogen (DON), including alkylamines, to both the ocean and the atmosphere, with notable release during sea-ice melt (Dall'Osto et al., 2017, 2019; Rinaldi et al., 2020) (Dall'Osto et al., 2017, 2019; Rinaldi et al., 2020).

Despite recent efforts, the quantification of these species in seawater remains a considerable challenge due to their low concentrations and reactivity (Fitzsimons et al., 2023) (Fitzsimons et al., 2023), which hampers understanding of their concentrations in both dissolved and particulate forms. In the ocean, the main alkylamines reported are the class of methylamines (MAs), which exist in primary (monomethylamine, MMA:  $\text{CH}_3\text{NH}_2$ ), secondary (dimethylamine, DMA:  $(\text{CH}_3)_2\text{NH}$ ), and tertiary (trimethylamine, TMA:  $(\text{CH}_3)_3\text{N}$ ) forms, plus diethylamine (DEA:  $(\text{CH}_3\text{CH}_2)_2\text{NH}$ ), a secondary amine with two ethyl groups bound to the amino nitrogen (N) (Goldwhite, 1964) (Goldwhite, 1964). Amine concentrations in seawater are determined by biogeochemical processes, including production and consumption by marine microorganisms (Gibb et al., 1999) (Gibb et al., 1999). Phytoplankton, other protists and bacteria release N-containing compounds such as proteins, amino acids and several forms of amines (Poste et al., 2014) (Poste et al., 2014) via organism excretion, cell death or lysis. Some of these compounds are directly synthesized by phytoplankton and used as osmolytes for regulating cellular homeostasis in response to salinity variations (Burg and Ferraris, 2008), and as cryoprotectants (Fitzsimons et al., 2024) (Burg and Ferraris, 2008), and as cryoprotectants (Fitzsimons et al., 2024). The precursors for alkylamines are glycine betaine, choline, trimethylamine N-oxide (TMAO), and quaternary amines ( $\text{R}_4\text{N}^+$ ). These N- (and Carbon, C) containing molecules are progressively degraded to TMA by bacteria, followed by further degradation into the less methylated compounds, DMA and MMA (Lidbury et al., 2015a, b; Matusz and Chen, 2019; Sun et al., 2019) (Lidbury et al., 2015a, b; Matusz and Chen, 2019; Sun et al., 2019). This displays similarities to the ocean sulfur cycle of DMSP and DMS (Stefels, 2000) dimethylsulfoniopropionate and dimethylsulfide (DMSP and DMS, respectively) (Stefels, 2000). Marine bacteria and archaea can

ha formattato: Colore carattere: Verde

use alkylamines as a source of energy and remineralize the organic N to ammonium (Landa et al., 2017; Lidbury et al., 2015a; Mausz and Chen, 2019). (Landa et al., 2017; Lidbury et al., 2015a; Mausz and Chen, 2019).

The few available studies showed that alkylamines represent a small and highly variable percentage of marine ON compounds in the ocean (Fitzsimons et al., 2023). (Fitzsimons et al., 2023, 2024 and references therein). The presence of alkylamines in seawater can have ecological implications, serving as nutrients (C and N sources) for marine microbiota, thereby influencing primary production and ecosystem dynamics (Chistoserdova et al., 2009; Palenik and Morel, 1991; Taubert et al., 2017). (Chistoserdova et al., 2009; Palenik and Morel, 1991; Taubert et al., 2017). For instance, in tropical waters van Pinxteren et al. (2019) van Pinxteren et al. (2019) found an association between alkylamines and biological tracers such as chlorophyll-a and fucoxanthin, suggesting that they were produced by marine diatoms. Furthermore, Koester et al. (2022) Koester et al. (2022) hypothesised that the broad array of N metabolites plays a significant role in the interactions between the diatom *Pseudo-nitzschia* and its bacterial microbiome (particularly *Polaribacter*), thus contributing fundamentally to the ecophysiology of the diatom. Also, Suleiman et al. (2016) Suleiman et al. (2016) showed that interactions between diatoms and heterotrophic bacteria may be important for marine amine cycling. Investigations into the co-occurrence and abundance of proteobacteria, diatoms and MAs in the marine water column have uncovered interkingdom cross-feeding, underscoring the previously underestimated significance of MAs in the marine N and C cycles (Stein, 2017). MAs also play a significant role in facilitating the bacterial conversion of the climate-relevant sulfur gas dimethylsulfide (DMS) into dimethylsulfoxide (DMSO) (Lidbury et al., 2016). (Stein, 2017). Moreover, MAs share a bacterial oxidation pathway with the climate-relevant sulfur gas DMS into dimethylsulfoxide (DMSO) (Lidbury et al., 2016). DEA has been previously found in seawater (Poste et al., 2014; Van Pinxteren et al., 2012, 2019; Fitzsimons et al., 2024) and marine aerosols (Facchini et al., 2008; Dall'Osto et al., 2019). However, no information exists on production pathways, potential biological precursors, or transformation processes in seawater. In summary, the amine cycle in the ocean is related to several microbial processes, which this study sought to explore further.

Here we aimed to investigate the presence, distribution, and potential sources of alkylamines in Antarctic waters and to enhance our understanding of how these compounds are linked to polar

ha formattato: Colore carattere: Automatico

microbial ecology. To achieve this, we visited the Southern Ocean near the Antarctic coasts, one of the most pristine environments on Earth, which is a source of ON (Dall'Osto et al., 2017) (Dall'Osto et al., 2017) and serves as a proxy for preindustrial marine conditions. Surface waters around the Antarctic Peninsula were analysed using a sensitive and robust method specifically designed for detecting low molecular weight aliphatic amines. We characterized in detail the biogeochemical properties and microbial composition of the same waters to explore the drivers of alkylamine distribution.

## 2 Methods and Material

### 2.1 Study Area and Sampling Strategy

The PolarChange (Aerosol Emissions in Changing Polar Environments) expedition was conducted on board the RV *Hesperides* in the Southern Ocean around the Antarctic Peninsula, during late austral summer from the 14<sup>th</sup> of February to the 17<sup>th</sup> of March 2024 (2023). During this cruise, we collected surface seawater samples from the underway water inlet (~4 m deep) to analyse for amines (dissolved and particulate forms) and accompanying microbiota and biogeochemical parameters. Seven stations were located in the western side of the Antarctic Peninsula, and 12 (twelve) in the eastern side, within the Weddell Sea area (Fig. 1, Table S1). Seawater was obtained at 18:00 (local time), except for samples #2 and #18, which were collected at 12:00 mid-day. Sea surface water temperature (°C) (SST), salinity and density (sigmaT) were measured by the probe SeaBird SB21 connected to the continuous system and surface solar radiation was measured by a radiometer located in the upper deck (model QCPRR-800) (PAR; W m<sup>-2</sup>).

### 2.2 Alkylamine Sampling and Analysis Protocol

Seawater was directly collected into 50 mL propylene tubes (Falcon type), which were completely filled. For dissolved amine analysis, seawater was filtered through a 47 mm GF/F filter (0.7 µm pore size) by gravity (ca. 60 minutes, filtration timing depended on the microbial biomass and particulate matter contained in the sampled water) and directly collected into a new 50 mL propylene tube until completely filled. This procedure minimised headspace (Akenga and Fitzsimons, 2024) as indicated by Akenga and Fitzsimons (2024). This filtered water was preserved with concentrated 37 % HCl (analytical grade) at 1 % (v/v) final concentration. The tube was tightly closed and stored in the dark at 4 °C until analysis. In turn, after filtration, the GF/F filter

was ~~allowed to naturally dry at room temperature and~~ stored in a 2 mL eppendorf tube at -80 °C for particulate amine analysis.

### 2.2.1 Analysis of ~~Alkylamines~~alkylamines in ~~Seawater-Headspace~~seawater by headspace- based Solid-solid-phase Microextraction and Gas-Chromatography chromatography with Nitrogen-Phosphorus Detectiondetection

Dissolved and particulate amines in seawater were analysed following ~~Akenga and Fitzsimons~~  
~~(2024)~~Akenga and Fitzsimons (2024). Briefly, the method comprises an online, automated  
headspace solid-phase microextraction step coupled with gas chromatography and nitrogen-  
phosphorus detection (HS-SPME-GC-NPD), optimising the method reported by ~~Cree et al.~~  
~~(2018)~~Cree et al. (2018). The new protocol has improved precision, throughput and confidence  
with advantages in sample collection, storage and transport, particularly from remote environments  
(Fitzsimons et al., 2023). A sample chromatogram is shown in Fig. S1.

Codice campo modificato

### 2.2.2 Reagents and ~~Labware~~labware

Methylamine standards, monomethylamine (MMA, 99 %), dimethylamine (DMA, 99 %),  
trimethylamine (TMA, 98 %) and diethylamine (DEA, 99 %) in hydrochloride form were  
purchased from Thermo Fisher, UK. Cyclopropylamine (CPA, 99 %), analytical grade HCl (37  
%), 10 M NaOH and analytical grade NaCl were from Thermo Fisher, UK. All glassware was  
soaked for 24 h in Decon solution (2 %, v/v) and rinsed with high-purity water (HPW; 18.2 MΩ  
cm), then soaked in HCl (10 %, v/v) for 24h, rinsed again with HPW and allowed to dry at room  
temperature- ~~(RT)~~.

### 2.2.3 Analysis of ~~Dissolved Alkylamines~~dissolved alkylamines

Dissolved amines, i.e., dMMA, dDMA, dTMA and dDEA stock standard solutions were prepared  
at 94.8, 59.4, 63.7 and 100 nM, respectively, after an accurate dissolution of their chloride salts in  
HPW. Stock solutions and working standards were acidified with concentrated HCl at a ratio of  
1:1000 v/v (acid:solution). Calibration solutions for dMMA, dDMA and dTMA analyses were  
prepared in the ranges 9.48–94.8, 5.94–59.4 and 6.37–63.7 nM, respectively and at 10–100 nM for  
dDEA. Aliquots (10 mL) of the solutions were pipetted into 20 mL autosampler glass vials  
(cleaned as indicated above) then saturated with NaCl (33 %). CPA was used as an internal

standard and was added to each vial at a final concentration of 20 nM. The pH of each standard solution was adjusted to > 13.0 through addition of 10 M NaOH solution (250 µL) and the vials were immediately sealed. At this point, alkylamines were converted to gaseous form and diffused into the headspace, where they were adsorbed into the SPME fibre. Blank samples were prepared with HPW and treated with NaCl and NaOH as described. Samples analyses were conducted ~6 months after collection. From each stored sample, three 10 mL aliquots were distributed in glass vials and treated analogously to the standards.

#### 2.2.4 Analysis of ~~Particulate Alkylamines~~particulate alkylamines

We also measured amines in particulates retained on ~~the~~GF/F filters after seawater filtration. ~~The filters (section 2.2). Analyses were treated with conducted ~6 months after sample collection. Prior to extraction, each filter was placed in a 20 mL autosampler glass vial and allowed to thaw inside the vial (one filter per vial). Subsequently, we added 250 µL of CPA to a (20 nM final concentration of 20 nM,) as internal standard and 500 µL of 10 M NaOH was then added, to liberate gaseous amines from, and the filters. It vial was tightly sealed. This treatment was assumed thatto volatilize the target analytes were liberated to into the vial headspace in the same way as a manner analogous to dissolved samples and particulate. Particulate amine concentrations were quantified using standard amine solutions, as described above. For each particulate sample, the GF/F filters were placed in 20 mL autosampler glass vials, allowed to defrost and CPA and NaOH were added directly onto the filter. previously.~~

#### 2.2.5 SPME and ~~Gas Chromatography~~gas chromatography

Details of the automated method are provided in ~~Akenga and Fitzsimons (2024)~~Akenga and Fitzsimons (2024). Briefly, the process involved extracting analytes onto an SPME fibre after equilibration in an integrated oven (60 °C), followed by injection of the SPME fibre into the GC (~~Gas Chromatography~~gas chromatography) system. Thermal desorption of the analytes occurred in the injector port (250 °C), followed by their separation and detection on a 60 m CP-Volamine column. Once separated, the analytes were detected by a nitrogen-phosphorus detector at 300 °C. The total run time ~~lasts~~lasted 25 minutes. Peak area data acquisition and processing was performed by ThermoChromeleon vs. 7.3 software. The three MAs and DEA were baseline resolved on the column and separated from CPA. The retention times of MMA, DMA, TMA, DEA and CPA were

ha formattato: Non Apice / Pedice



7.2, 8.1, 8.6, 12.0 and 11.3 minutes, respectively (Fig. S1). An  $R^2$  value  $>0.90$  was achieved for the calibration of the four alkylamines. The ~~calculated~~ limits of detection for MMA, DMA, TMA and DEA, were 9.5, 5.9, 1.1 and 4.3 nM, respectively. Additionally, the ~~dissolved~~ calibration curve for ~~dissolved~~ TMA was used to detect particulate TMA values.

## 2.3 Biological Parameters

### 2.3.1 Chlorophyll-a

Between 200 and 750 mL of seawater were filtered through 25 mm Whatman GF/F glass fibre filters to estimate the total chlorophyll-a concentration. All filters were stored at  $-20\text{ }^{\circ}\text{C}$  until analyses ~~conducted~~ on board the *R/V Hesperides*. Chlorophyll-a (Chl-a) concentrations were estimated fluorometrically after extraction in 90 % acetone at  $4\text{ }^{\circ}\text{C}$  ~~for 24h (Yentsch and Menzel, 1963).~~  $^{\circ}\text{C}$  ~~for 24h (Yentsch and Menzel, 1963).~~ Readings were conducted on a Turner 10AU fluorimeter calibrated with pure chlorophyll extract from spinach (Sigma C5357) using a Beckton-Dickinson spectrophotometer. A Carbon:Chlorophyll ratio of 50 ~~(Jakobsen and Markager, 2016)~~ ~~was applied (Jakobsen and Markager, 2016)~~ was applied to estimate the phytoplankton biomass in terms of Carbon.

### 2.3.2 Viral and ~~Bacterial Abundance~~ bacterial abundance and ~~Biomass~~ biomass

Subsamples (2 mL) were fixed with glutaraldehyde (0.5 % final concentration) for viruses, and with 1 % paraformaldehyde + 0.05 % glutaraldehyde for bacteria estimations by flow cytometry (FCM). After 15–30 min in the dark at  $4\text{ }^{\circ}\text{C}$ , the fixed samples were flash-frozen in liquid nitrogen and subsequently stored at  $-80\text{ }^{\circ}\text{C}$ . ~~Viral (Brussaard, 2004) and bacterial (Gasol and Del Giorgio, 2000) until analysis. Viral (Brussaard, 2004) and bacterial (Gasol and Del Giorgio, 2000)~~ abundances were measured in a Cytoflex flow cytometer at the ICM-CSIC laboratory (up to 5 months after sampling). Samples for viral abundance were ~~thawed and~~ diluted with TE-buffer (10:1 mM Tris: EDTA), stained with 50x SYBR Green I to a final concentration of 1 %, heated in a  $80\text{ }^{\circ}\text{C}$   ~~bath for 10 min and run at a constant flow rate of  $60\text{ }\mu\text{L min}^{-1}$  according to Brussaard (2004).~~ Brussaard (2004). Viruses were determined in bivariate scatter plots of the green fluorescence of stained nucleic acids *versus* side scatter. Based on their green fluorescent and side scatter signals, four distinct virus populations (V1–V4) were identified (Fig. S2). Presumably, V1 and V2 populations are dominated by bacteriophages ~~(Biggs et al., 2021)~~ (Biggs et al., 2021); the

V3-V4 fractions by eukaryotic algal viruses (~~Evans et al., 2009~~)(Evans et al., 2009), and V4 fraction correspond primarily to Haptophyceae (e.g., *Phaeocystis* spp.) viruses (~~Brussaard et al., 1999, 2005; Rocchi et al., 2022~~)(Brussaard et al., 1999, 2005; Rocchi et al., 2022). Virus biomass was calculated ~~from using~~ the carbon virus content ~~factor~~ of 0.2 fg C/fgC virus<sup>-1</sup> (~~Suttle, 2005~~)(Suttle, 2005). Thawed samples for bacterial abundance were stained with 50x SYBR Green I at a final 1 % concentration and incubated for 5 min in the dark. Based on the flow cytometer side scatter *versus* green fluorescence (FL1) signatures, high nucleic acid (HNA) from low nucleic acid (LNA) content bacteria were identified (~~Gasol and Del Giorgio, 2000~~)(Gasol and Del Giorgio, 2000) (Fig. S3). Bacterial biomass was obtained from the carbon-to-volume relationship (~~Norland, 1993~~)(Norland, 1993) namely,  $\text{pg C/pgC cell}^{-1} = 0.12 \times V^{0.7}$ , where V is the bacteria volume cells in  $\mu\text{m}^3$ . Here, an average cell volume of 0.066  $\mu\text{m}^3$  bacteria<sup>-1</sup> reported for Antarctic waters (Vaqu   et al., 2004) was used.

Codice campo modificato

### 2.3.3 Pico- and Nanophytoplankton ~~Abundance~~nanophytoplankton abundance and Biomass~~biomass~~

Samples for photosynthetic pico- and nanophytoplankton abundances ~~were collected on 5 mL cryovials, fixed with glutaraldehyde (1% final concentration) and frozen in liquid nitrogen following Vaultot et al. (1989). Cells~~ were counted by a CyFlow Cube 8 flow cytometer (Sysmex) at the ICM-CSIC. Phytoplankton cells were detected with a 488 nm laser beam from their signatures in a plot of side scatter (SSC) *versus* ~~green~~red fluorescence (FL3), separating the picophytoplankton ~~fraction size class~~ of 1–2  $\mu\text{m}$  (sphere equivalent diameter, SED), ~~and the nanophytoplankton fractions of size classes with SEDs of 2–7  $\mu\text{m}$ , 7–15  $\mu\text{m}$ , and 15–20  $\mu\text{m}$  (Fig. S4).~~ Within the nanophytoplankton, Cryptophytes ~~size classes~~ (*Cryptomonas* spp.) (~~Fig. S4~~) ~~were identified by their phycoerythrin signal in the FL3 vs orange fluorescence (FL2) plots (Marie et al., 2014).~~ Biomasses ( $\mu\text{g C L}^{-1}$ ) of these cell sizes were measured using the formula,  $\text{pg C/pgC cell}^{-1} = 0.216 \times V^{0.939}$  (V, cell volume; ~~Menden-Deuer and Lessard, 2000~~)(Menden-Deuer and Lessard, 2000). The phytoplankton cell volume varied between 1.8 and 63  $\mu\text{m}^3$  cell<sup>-1</sup>.

### 2.3.4 Nanoflagellate ~~Abundance~~abundance and Biomass~~biomass~~

Abundances of heterotrophic and phototrophic nanoflagellates, including *Phaeocystis*, in the size fraction 2–20  $\mu\text{m}$  (SED) were determined by epifluorescence microscopy (~~Olympus BX40-102/E~~

at 1000X). Subsamples of 30 mL were taken from seawater; samples were fixed with glutaraldehyde (1 % final concentration), filtered through 0.6 µm black (25 mm diameter) polycarbonate filters, and stained with 4,6-diamidino-2-phenylindole (DAPI) at a final concentration of 5 µg mL<sup>-1</sup> (Sieracki et al., 1985). Under blue light, concentrations of filters were placed on slides and kept frozen (-20 °C). Microscope cell counts of heterotrophic (HNF) and phototrophic nanoflagellates (PNF) were estimated by the fluorescence response of the cells after blue light illumination using an Olympus BX40-102/E at 1000X epifluorescence microscope. PNFs were distinguished by the observation of red fluorescence emitted by photosynthetic plastid structures, while HNF were identified from the yellow fluorescence of DAPI stained nuclei. At least 50 HNFs and 50 PNFs were counted per sample (3 transects of 5 mm in each filter) and classified into ≤ 2 µm, 2–5 µm, 5–10 µm, and 10–20 µm size (SED) classes. The nanoflagellate carbon cell content was estimated from the corresponding carbon-to-volume ratio, e.g., pgC cell<sup>-1</sup> = 0.216 x (V)<sup>0.939</sup> (Menden-Deuer and Lessard, 2000) (Menden-Deuer and Lessard, 2000), where the cell volume (V) was calculated from the average length of each nanoflagellate cell size class and transformed into spherical or ellipsoidal volume. The nanoflagellate cell volume varied between 1.8 and 57.6 µm<sup>3</sup> cell<sup>-1</sup>.

### 2.3.5 Microplankton Assemblages

The microplankton community was characterised using the Utermöhl method on 125 mL neutral lugol fixed seawater samples. 50 mL aliquots samples were settled in sedimentation chambers for 24 h and observed in a Leica MDi1 inverted microscope (Edler and Elbrächter, 2010) (Edler and Elbrächter, 2010). The identified taxa and size classes included: dinoflagellates (resting cysts, vegetative dinoflagellates 10–20 µm, 20–40 µm, and > 40 µm), diatoms (10–20 µm, 20–40 µm, and > 40 µm) and ciliates. When possible, taxa were identified at the genus and species level. The relative biomasses (in µg C µgC L<sup>-1</sup>) were measured from cell volumes using the Cell C-carbon-to biovolume-volume relationships estimated by Menden-Deuer and Lessard (2000) (Menden-Deuer and Lessard (2000) on diatoms and dinoflagellates. Namely, the equation pgC cell<sup>-1</sup> = 0.760 x (µm<sup>3</sup> cell<sup>-1</sup>)<sup>0.819</sup> was used for dinoflagellates and pgC cell<sup>-1</sup> = 0.288 x (µm<sup>3</sup> cell<sup>-1</sup>)<sup>0.811</sup> for diatoms. Cell volume was calculated using a geometric formula on cell length and width measurements conducted using a digital camera and specific calibration of the used Leica DMi1 microscope. The biovolume was estimated considering an ovoid, a cylinder or a prism shape for dinoflagellates,

centric diatoms, and pennate diatoms, respectively. ~~The estimation of the cell volume is referred to the main cell body dimension, and empty sphere for empty dinoflagellate cysts. Cell dimensions measurements (excluding chaetae and other cell expansions-) were conducted using a digital camera and specific calibration of the used Leica DMi1 microscope.~~ Empty diatom frustules were assumed to have a null contribution to C.

### 2.3.6 Photosynthetic ~~Efficiency~~efficiency

The relative efficiency of excitation energy captured by the photosystem II (PSII), calculated as  $F_v'/F_m'$ , is used as a proxy of phytoplankton stress and fitness ~~(Gorbunov et al., 2020; Gorbunov and Falkowski, 2022).~~(Gorbunov et al., 2020; Gorbunov and Falkowski, 2022). The metric is measured by a multi-color fluorescence induction and relaxation instrument (mini-FIRE) ~~(Gorbunov et al., 2020) system~~ (Gorbunov et al., 2020). The instrument records two parameters:  $F_0'$  as the minimal yield of fluorescence before fast light flashes, and  $F_m'$ , the maximum yield of fluorescence due to the reradiation of the maximum number of photons. The difference between  $F_m'$  and  $F_0'$  is called variable fluorescence ( $F_v'$ ). The quotient of  $F_v'/F_m'$  represents the effective photosynthetic efficiency of the community measured under light conditions ~~(Gorbunov and Falkowski, 2022).~~(Gorbunov and Falkowski, 2022).  $F_v'/F_m'$  has no units, so that it is independent of the phytoplankton abundance and allows comparisons between environments. Aliquots of 10 mL were sampled from the underway system and rapidly placed in the chamber of the mini-FIRE to apply the induction and relaxation protocol for dilute samples. No dark acclimation period was used. ~~A hundred acquisitions were averaged for each sample using the fview software and the resulting data was processed with the fprope software to obtain all the desired parameters.~~

## 2.4 Chemical ~~Parameters~~parameters

### 2.4.1 Particulate Organic Carbon and Nitrogen

Particulate organic carbon (POC) and nitrogen (PON) content in the seawater was determined by filtration of ~~250~~390 to 1000 mL through pre combusted (450 °C, 4h) 25mm GF/F glass fibre filters (Whatman) at low pressure (<20mmHg) and kept frozen (-80 °C) until analysis. Filters were thawed and dried at RT, exposed to 37 % (pure) HCl atmosphere in a hermetic beaker to eliminate carbonate salts and subsequently analysed with an Elemental Analyser (Perkin-Elmer 2400 CHN)

ha formattato: Barrato

Formattato: SpazioDopo: 12 pt, Interlinea: 1.5 righe

at the Scientific and Technical Service of the University of Barcelona. In the following, the term POC and PON will refer to the C and N estimated biochemically as described here as a proxy of particulate organic matter, consisting in living and non-living cells, extracellular material and detritus containing C or N.

#### 2.4.2 Dissolved Carbon and Nitrogen

For total organic carbon (TOC) and nitrogen (TN: organic and inorganic nitrogen) analyses, 30 mL of seawater was filtered through a HCl clean 200 µm mesh by gravity and collected in polycarbonate bottles. The sample was fixed with 100 µl of 25 % H<sub>3</sub>PO<sub>4</sub> stored frozen (-20 °C) until analysis in the laboratory. Following the elimination of inorganic C (i.e., carbonates) by the acidification of the sample, determination of TOC and TN in seawater was conducted by high temperature catalytic oxidation (680 °C and 720 °C, respectively) as described in [Álvarez-Salgado and Miller \(1998\)](#). Measurements were conducted with the TOC-L Shimadzu autoanalyzer, with deep Sargasso Sea water used as control (Hansell Laboratory, University of Miami, RSMAS). Concentrations are expressed as µM (µmol C L<sup>-1</sup> or µmol N L<sup>-1</sup>). Dissolved Organic Carbon (DOC) and Nitrogen (DON) were calculated by subtraction of POC from TOC, and nitrate, nitrite, ammonium and PON concentrations from TN, respectively.

#### 2.4.3 Dissolved ~~Inorganic Nutrient Analysis~~inorganic nutrient analysis and ~~Total~~total Phosphorus

For ~~estimation~~measurements of nutrient concentrations, seawater samples were collected in two different 50 mL polypropylene plastic tubes: one tube was used for the determination of inorganic nutrients (nitrate, nitrite, ammonium, phosphate and silicate) and the other one for total phosphorus (TP, organic and inorganic forms). Samples were immediately frozen and stored at -20 °C until analysis. ~~Determinations~~Concentrations of inorganic nutrients were ~~estimated~~determined with an AA3 HR autoanalyzer (Seal Analytical) and TP with an AA3 autoanalyzer after previous digestion, following [Grasshoff et al. \(1983\)](#).

#### 2.4.4 Total ~~Dimethylsulfoniopropionate~~dimethylsulfoniopropionate (DMSP) ~~Concentrations~~concentrations

ha formattato: Colore carattere: Automatico

Codice campo modificato

Samples for total DMSP (DMSPt) ~~estimation~~analysis were collected directly from the underway system on ~30 mL borosilicate serum vials and processed following ~~Kinsey and Kieber (2016)~~Kinsey and Kieber (2016). The vials were uncapped and individually heated by microwave until they began to boil. After the first bubble formed, the microwave was stopped and the vial was left to cool. Subsequently, 30 µl of 37 % HCl were added to all the vials to remove the DMS present and preserve the DMSP. Acidified samples were stored at RT in the dark. Within six months of the cruise, DMSP was converted to DMS by alkaline hydrolysis with NaOH for at least 24 hours. The resulting DMS was quantified with a cryogenic purge-and-trap system coupled to a Thermo Fisher TRACE 1300 gas chromatograph with flame photometric detection following ~~Masdeu-Navarro et al. (2022)~~Masdeu-Navarro et al. (2022).

#### 2.4.5 DMS measurements by ~~Vocus~~Proton Transfer Reaction Time-of-Flight Mass Spectrometry (PTR-ToF-MS)

A Vocus-PTR-ToF-MS coupled to a segmented flow coil equilibrator was used to continuously measure seawater dissolved DMS (~~Wohl et al., 2019~~)(Wohl et al., 2019). An overview on operation and calibrations is provided in Wohl et al. (2024).

#### 2.5 Statistical ~~Analyses~~analyses

All analyses were conducted in the RStudio integrated development environment (RStudio Team, 2023) to ensure reproducibility and clarity. Multivariate statistical analyses were performed using R version 4.3.2 (R Core Team, 2023) to explore relationships among variables. The data were normalised by centering and scaling to ensure equal contribution of all variables to the Principal Component Analysis (PCA). The PCA was conducted to reduce dimensionality and examine the relationships among variables. The analysis employed the princomp() function from the stats package (Bolar, 2019), using the correlation matrix of normalized data as input to focus on inter-variable relationships. Visualizations were generated using the factoextra package version 1.0.7 (~~Kassambara and Mundt, 2020~~)(Kassambara and Mundt, 2020). The ggcorrplot package (Kassambara, 2021) was used to create a heatmap of variable correlations, while the gridExtra package (~~Auguie, 2017~~)(Auguie, 2017) facilitated side-by-side comparisons of variable contributions to principal components. Factor Analysis was performed to uncover latent structures within the dataset using the psych package version 2.3.6 (~~Revelle, 2023~~)(Revelle, 2023). Factor

Codice campo modificato

383 extraction employed Principal Axis Factoring with Varimax rotation to achieve interpretability,  
384 complemented by Maximum Likelihood Estimation for comparison. Factor loadings were  
385 visualized using ggplot2 version 3.4.4 (Wickham, 2023). Mantel Test was used  
386 to assess the correlation between two distance matrices using the vegan package version 2.6-4  
387 (Oksanen, 2022). For each pair of variables, Euclidean distance matrices were computed and tested  
388 for significant Pearson correlations. Results with p-values < 0.05 were considered significant. The  
389 Wilcoxon test and ggplot2 were used to analyze and visualize statistical differences between the  
390 Antarctic Peninsula and Weddell Sea groups, with a logarithmic y-axis improving data  
391 interpretation.

392

### 393 3 Results

#### 394 3.1 Cruise setting

395 The regional satellite images of SST and Chlorophyll concentration during the cruise period (Fig.  
396 1) indicates two ~~well-defined~~distinct areas where the PolarChange cruise was conducted: the  
397 Western Antarctic Peninsula and the northern Weddell Sea. For this reason, in the following we  
398 will explore potential differences between these two areas concerning biological and biochemical  
399 parameters (Fig. S5). Sea surface temperature (SST) ranged between  $-0.67$  and  $2.04$  °C (Table S1)  
400 with statistical differences within the two studied marine areas, (average  $\pm$  SD values)  $1.9 \pm 0.6$   
401 °C (n=7) in the western part of the Antarctic Peninsula compared to the colder waters of the  
402 Weddell Sea with  $0.2 \pm 0.7$  °C (n=12; p=0.0072) (Table S1 and Fig. S5). Salinity (Table S1)  
403 remained relatively constant throughout the expedition, averaging  $33.9 \pm 0.3$ . Concerning solar  
404 irradiance (Table S1), higher but not significantly different values were observed near the  
405 Antarctic Peninsula,  $355 \pm 257$  W m<sup>-2</sup>, compared to the  $226 \pm 194$  W m<sup>-2</sup> numbers observed in the  
406 Weddell Sea.

Formattato: SpazioPrima: 10 pt



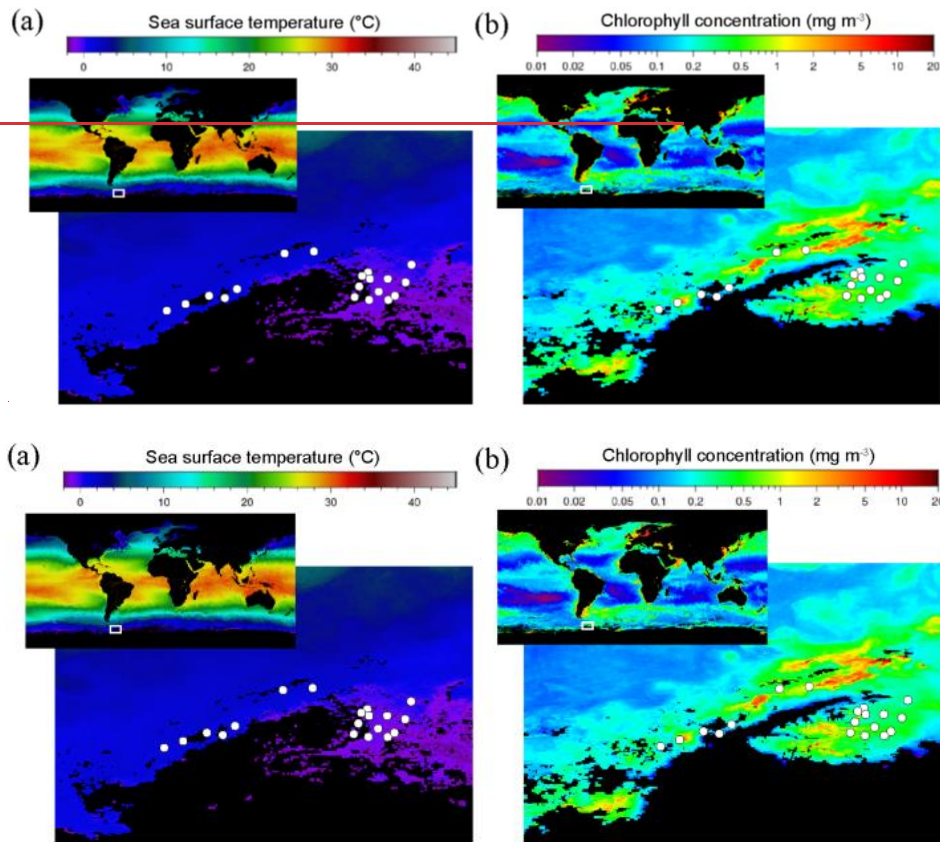


**Figure 1.** Satellite images of (a) the sea surface temperature and (b) the chlorophyll distribution in the ocean (small upper insert) with a zoom in the Southern Ocean around the Antarctic Peninsula and the Weddell Sea in March 2023 during the period of the ~~Polar-Change~~PolarChange cruise ~~when most amine samples were collected~~. White circles indicate the location of the 19 stations where all samples analysed in this study were collected (the first seven stations are located in the Western Antarctic Peninsula, while the remaining twelve stations are situated in the Weddell Sea; see stations list in Table S1). Chlorophyll concentration is estimated from the Ocean Color Index (OCI) Algorithm and the sea surface temperature from SNPP VIIRS satellite, <https://oceancolor.gsfc.nasa.gov/13/>.

### 3.2 Alkylamine concentrations

#### 3.2.1 Dissolved ~~Alkylamines~~alkylamines

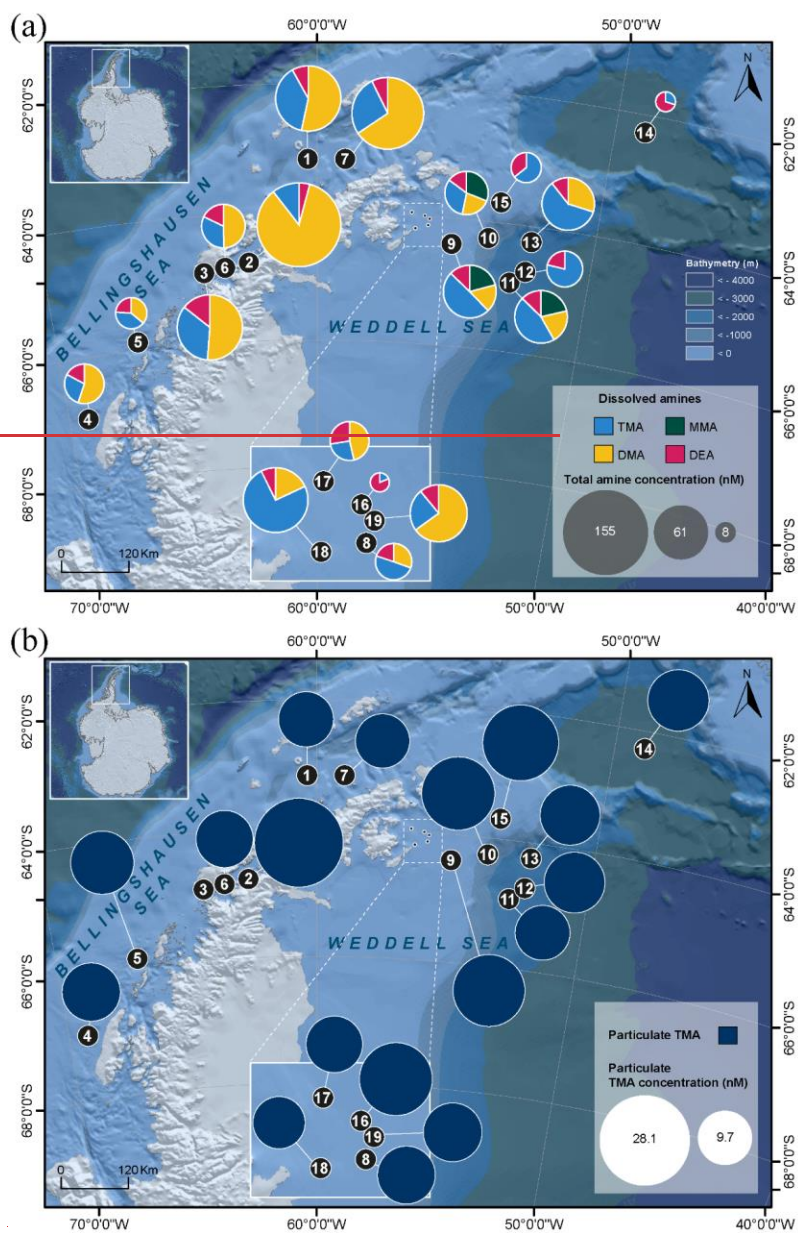
We detected dissolved MAs and DEA at ~4 m of depth over the cruise (Fig. 2a and Table S1). Dissolved MMA (~~dMMA~~) was quantitatively ~~estimated~~identified only in samples #9, #10, #11 in



the Weddell Sea with an overall concentration average of  $12.7 \pm 0.1$  nM (n=3). With this method we could detect dDMA in most of the samples, ranging from 7.6 nM to 132.3 nM with an average of  $32.3 \pm 32.7$  nM (n=15); it was below detection limits in samples #12, #14, #15, #16. The concentration of dDMA was statistically higher near the Antarctic Peninsula compared to the Weddell Sea (respectively,  $49.9 \pm 39.6$  nM, n=7 and  $17.0 \pm 11.4$  nM, n=8; p=0.04) (Fig. S5). dTMA was measured in all the samples varying from 1.485 nM to 67.9 nM with an average of  $20.9 \pm 15.2$  nM (n=19) ( $20.8 \pm 10.6$  nM, n=7 for the Western Antarctic Peninsula and  $21.0 \pm 17.3$  nM, n=12 for the Weddell Sea; p=0.77). dDEA was identified in all the samples but with lower concentrations than the dissolved MAs along the studied area (Table S1). ~~It had a more even distribution, with~~ dDEA concentrations ~~rangingranged~~ between 5.1 nM and 13.3 nM, ~~andwith~~ an average of  $7.2 \pm 1.7$  nM (n=19) ( $7.7 \pm 2.5$  nM, n=7 for the Western Antarctic Peninsula and  $6.9 \pm 1.0$  nM, n=12 for the Weddell Sea; p=0.77). In this study, dDEA had the most even distribution of all alkylamines (excluding dMMA), with a coefficient of variation of 23 %, compared to 101 % for dDMA and 73 % for dTMA.

### 3.2.2 Particulate ~~Alkylamines~~alkylamines

Only pTMA was detected and identified (Fig. 2b and Table S1) in 18 filter samples (sample #3 was lost), i.e., associated with particles. pTMA showed concentrations ranging between 9.7 nM and 28.1 nM with an average of  $14.4 \pm 4.6$  nM ( $14.5 \pm 6.2$  nM, n=6 for the Western Antarctic Peninsula and  $14.4 \pm 3.6$  nM, n=12 for the Weddell Sea; p=0.62).



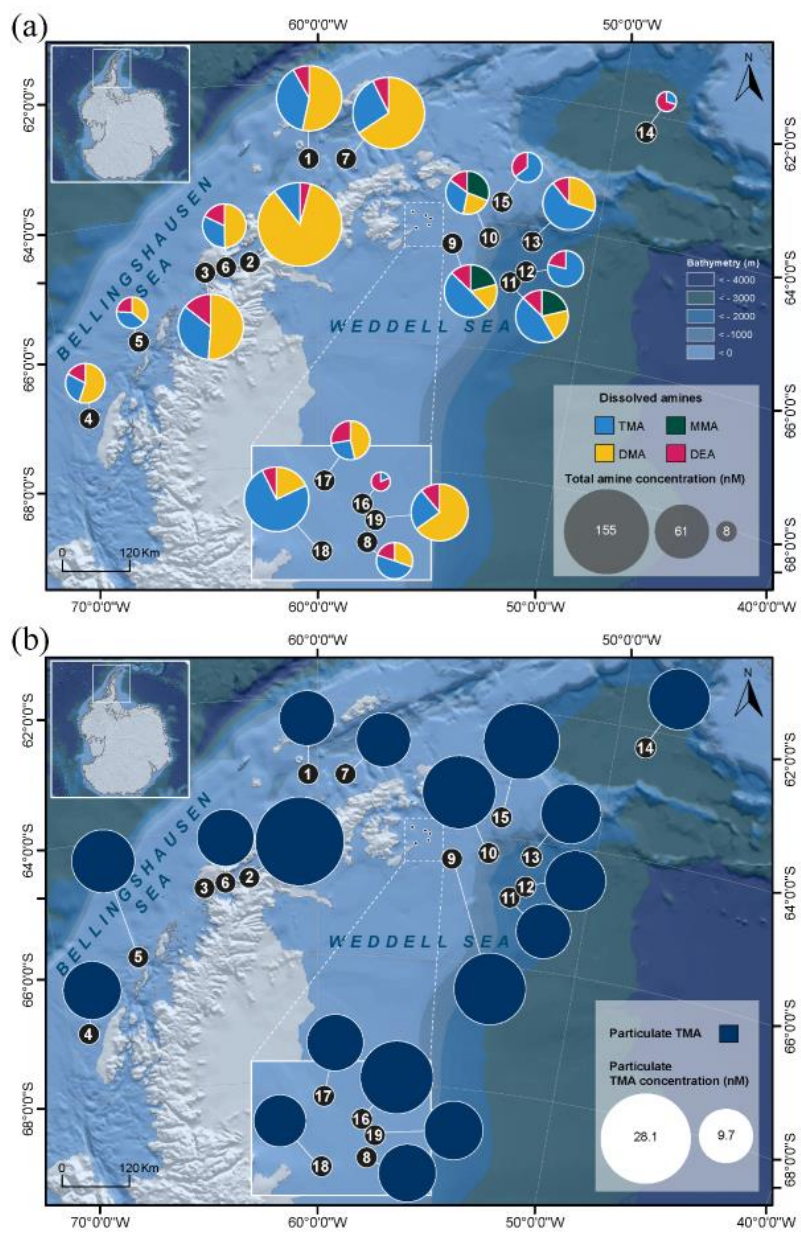


Figure 2. Distribution of the concentrations (using pie charts) of (a) the four dissolved alkylamines (MMA, DMA, TMA and DEA) and (b) particulate TMA (\*note that the particulate sample #3 was lost) in the studied area.

### 3.3 Biological Variables

#### 3.3.1 Chlorophyll-a Concentrations

The Chl-a concentrations varied along the oceanographic cruise, from 0.2 to 9.6  $\mu\text{g L}^{-1}$ , throughout the area (Fig. 1), with an average of  $1.2 \pm 2.0 \mu\text{g L}^{-1}$  (n=19) (Table S2). More productive waters were found in the western side of the Antarctic Peninsula, with an average of  $2.5 \pm 2.9 \mu\text{g L}^{-1}$  (n=7) significantly higher than the values estimated/observed in the Weddell Sea samples ( $0.5 \pm 0.3 \mu\text{g L}^{-1}$ , n=12; p=0.0077) (Fig. S5).

#### 3.3.2 Viral and Bacterial Abundances

Viral abundances (VA) (Table S2) averaged  $8.2 \pm 3.8 \times 10^6$  viruses  $\text{mL}^{-1}$  (n=19) and the V1, V2 and V3 populations accounted, on average and respectively, for the 80 %, 16.5 % and 3.5 % of total VA. V4 was only present in sample #15 with an abundance of  $1.8 \times 10^5$  viruses  $\text{mL}^{-1}$ . On average, total VA was slightly but significantly higher near the Antarctic Peninsula ( $11.5 \pm 3.8 \times 10^6$  viruses  $\text{mL}^{-1}$ , n=7) than in the Weddell Sea ( $6.2 \pm 1.9 \times 10^6$  viruses  $\text{mL}^{-1}$ , n=12; p=0.013) (Table S2 and Fig. S5). V1 abundance was also significantly higher in the Antarctic Peninsula ( $9.4 \pm 3.1 \times 10^6$  viruses  $\text{mL}^{-1}$ , n=7) than in the Weddell Sea ( $4.9 \pm 1.7 \times 10^6$  viruses  $\text{mL}^{-1}$ , n=12; p=0.0098) (Table S2 and Fig. S5). Concerning bacterial abundances (BA), the total average was  $6.4 \pm 2.5 \times 10^5$  cells  $\text{mL}^{-1}$  (n=19) with slightly (but not significantly different) higher numbers in the waters near the Antarctic Peninsula ( $7.0 \pm 1.6 \times 10^5$  cells  $\text{mL}^{-1}$ , n=7) compared to Weddell Sea ( $6.0 \pm 2.8 \times 10^5$  cells  $\text{mL}^{-1}$ , n=12). However, the highest value was estimated in sample #16 ( $11.7 \times 10^5$  cells  $\text{mL}^{-1}$ ) (Table S2) collected in the Weddell Sea. Generally, most bacteria had a high nucleic acid content, indicating that more than half of the total bacteria numbers were active cells (Table S2). Note that here, we are referring to cell abundances and not to biomass; C concentration values estimated/calculated from cell numbers followed the same patterns as cell abundances for each microorganism described (data not shown in the text, see SI).

#### 3.3.3 Pico- and Nanophytoplankton Abundances

Regarding phytoplankton measured by FCM, the abundances of the five identified groups (1–2  $\mu\text{m}$ , 2–7  $\mu\text{m}$ , 7–15  $\mu\text{m}$ , 15–20  $\mu\text{m}$  and Cryptophytes) were  $1.6 \pm 1.7 \times 10^3$ ,  $1.8 \pm 0.6 \times 10^3$ ,  $5.7 \pm$

7.5 × 10<sup>2</sup>, 1.3 ± 2.5 × 10<sup>2</sup>, 1.5 ± 2.5 × 10<sup>2</sup> cells mL<sup>-1</sup>, respectively (average ± SD values, n=19; Table S2). Picophytoplankton cells, ranging from 1 to 2 µm in size, exhibited significantly higher abundances around the Antarctic Peninsula, with an average of 3.3 ± 1.8 × 10<sup>3</sup> cells mL<sup>-1</sup> (n=7), compared to the Weddell Sea (6.1 ± 4.1 × 10<sup>2</sup> cells mL<sup>-1</sup>, n=12; p<0.001) (Fig. S5). Conversely, the average abundance of the larger cells, nanophytoplankton, ranging from 2 to 20 µm, appeared marginally higher in the Weddell Sea (2.7 ± 0.9 × 10<sup>3</sup> cells mL<sup>-1</sup>, n=12) than in the western part of the Antarctic Peninsula (2.2 ± 1.5 × 10<sup>3</sup> cells mL<sup>-1</sup>, n=7). Specifically, the abundance of ~~phytoplankton~~nanophytoplankton cells 2–7 µm in size was significantly greater in the Weddell Sea compared to the Antarctic Peninsula coasts (2.1 ± 0.5 and 1.3 ± 0.5 × 10<sup>3</sup> cells mL<sup>-1</sup>, n=19; p=0.0072) (Fig. S5). Similarly, cryptophytes (*Cryptomonas* spp.) presented abundances of 112 ± 143 cells mL<sup>-1</sup> (n=7) in the Western Antarctic Peninsula in contrast to 146 ± 121 cells mL<sup>-1</sup> (n=12) in the Weddell Sea.

### 3.3.4 Nanoflagellate ~~Abundances~~abundances

Abundances of HNF and PNF measured by epifluorescence microscopy were, on average, of 986 ± 951 cells mL<sup>-1</sup> and 5046 ± 2538 cells mL<sup>-1</sup> (n=15; samples #5, #9, #11 and #15 were lost), respectively (Fig. 3 and Table S3). In the Western Antarctic Peninsula, the abundances were 1234 ± 1195 cells mL<sup>-1</sup> for HNF and 4240 ± 1688 cells mL<sup>-1</sup> for PNF (n=6). In comparison, in the Weddell Sea, the abundances were 820 ± 698 cells mL<sup>-1</sup> for HNF and 5583 ± 2849 cells mL<sup>-1</sup> (n=9) for PNF. Concerning size, in the case of HNF, the ~~"intermediate" category, ranging from 2 to 5 µm~~group, constitutes the largest proportion of total abundance followed by the smallest size category (≤ 2 µm), the 5 to 10 µm group, and finally, the largest category ranging from 10 to 20 µm. Similarly, for PNF, the smallest size categories (≤ 2 µm and 2–5 µm) were the most abundant, followed by the 5–10 µm category, and lastly, the largest category spanning 10 to 20 µm (Fig. S5 Table S3). PNF 5–10 µm showed a statistical difference between the two Antarctic areas with barely higher concentrations in the Weddell Sea (117.3 ± 88.3 and 193.6 ± 74.4 cells mL<sup>-1</sup>, n=15; p=0.045) (Fig. S5). Total PNF exhibited slightly greater abundances in the Weddell Sea. Additionally, *Phaeocystis* presented slightly lower abundances west of the Antarctic peninsula of 208 ± 169 cells mL<sup>-1</sup> (n=6) in contrast to 352 ± 383 cells mL<sup>-1</sup> (n=9) in the Weddell Sea (Table S3).

ha formattato: Colore carattere: Testo 1

ha formattato: Colore carattere: Testo 1

ha formattato: Colore carattere: Testo 1

ha formattato: Colore carattere: Testo 1

ha formattato: Colore carattere: Testo 1

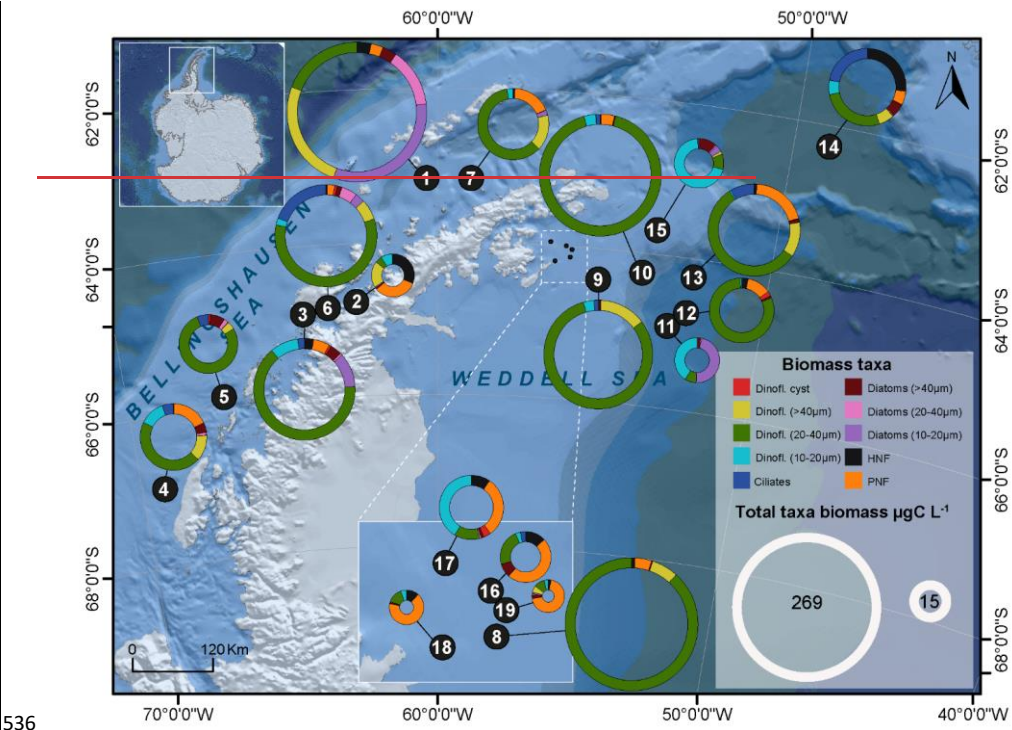
### 3.3.5 Composition and ~~Abundance~~abundance of ~~Microplankton Assemblages~~microplankton assemblages

A diverse range of phytoplankton taxa was found in the studied period in the Antarctic marine environments (Fig. 3 and Table S4). In the smallest size of the dinoflagellate group (10–20 µm), the identified taxa were *Gymnodinium* spp., Kareniaceae, *Oxytoxum* spp. and *Prorocentrum cordatum* (= *P. minimum*). The intermediate size group (20–40 µm) included larger taxa such as *Gymnodinium* spp., *Protoperidinium bipes*, *Gyrodinium* spp., Kareniaceae cells, and *Lebouridinium glaucum* (= *Katodinium glaucum*). In the >40 µm category, only *Gyrodinium* spp. and *Gymnodinium* spp. heterotrophs were present. Among diatoms, in the 10–20 µm size group, we identified a variety of genera, including centric and pennate chains, *Thalassiosira*, *Porosira*, *Coscinodiscus*, *Fragilaria*, *Chaetoceros* and *Amphora*. In the 20–40 µm size range, larger cells of *Coscinodiscus*, *Corethron criophilum* and its spores, pennate chains like *Pseudo-nitzschia*, *Proboscia alata*, *Licmophora*, *Achnanthes*, *Navicula*, *Leptocylindrus*, and *Actinocyclus* were observed. Among the larger diatoms (>40 µm), we identified *Coscinodiscus*, *Corethron criophilum*, and *Chaetoceros* spp., *Proboscia alata*, *Lioloma* chains, *Rhizosolenia curvata*, *Actinocyclus* and pennate diatoms. Non-photosynthetic taxa included mainly tintinnid ciliates.

Dinoflagellates were particularly dominant, though in general, they were distributed close to the Antarctic Peninsula. Specifically, dinoflagellate cysts accounted for ca.  $1.2 \pm 1.1 \times 10^3$  cells L<sup>-1</sup> (n=7), compared to  $0.8 \pm 1.6 \times 10^3$  cells L<sup>-1</sup> in the samples from the Weddell Sea (n=12). Dinoflagellates 10–20 µm were found at concentrations of  $6.9 \pm 5.8 \times 10^3$  cells L<sup>-1</sup> (n=7) near the Antarctic Peninsula, compared to  $1.3 \pm 1.2 \times 10^4$  cells L<sup>-1</sup> (n=12) in the Weddell Sea. Intermediate-sized dinoflagellates (20–40 µm) had similar abundances in both seas, with  $9.7 \pm 5.1 \times 10^3$  cells L<sup>-1</sup> in the Antarctic Peninsula waters (n=7) and  $1.7 \pm 2.3 \times 10^4$  cells L<sup>-1</sup> in the Weddell Sea (n=12). Larger dinoflagellates (>40 µm) were more concentrated in the Antarctic Peninsula waters, with  $1.2 \pm 1.4 \times 10^3$  cells L<sup>-1</sup> (n=7) compared to  $3.2 \pm 4.9 \times 10^2$  cells L<sup>-1</sup> (n=12) in the Weddell Sea. ~~In contrast~~Similarly, diatoms were more abundant near the Antarctic Peninsula waters: smaller diatom cells (10–20 µm) were significantly more prevalent in this area ( $2.0 \pm 3.7 \times 10^5$  cells L<sup>-1</sup>, n=7) compared to the Weddell Sea ( $4.7 \pm 9.1 \times 10^5$  cells L<sup>-1</sup>, n=12; p=0.0087) (Fig. S5). Furthermore, sample #1 exhibited the highest abundance of diatoms within the 10–40 µm size range compared to all other samples (Fig. 3). Intermediate-sized diatoms followed a similar



530 pattern, with  $1.2 \pm 2.9 \times 10^5$  cells  $L^{-1}$  (n=7) near the Antarctic Peninsula waters and  $6.7 \pm 8.5 \times 10^2$   
 531 cells  $L^{-1}$  (n=12) in the Weddell Sea. Larger diatoms ( $>40 \mu m$ ) presented slightly significantly  
 532 higher concentrations ( $3.5 \pm 2.9 \times 10^3$  cells  $L^{-1}$ , n=7) in the Antarctic Peninsula area than ( $8.0 \pm$   
 533  $5.8 \times 10^2$  cells  $L^{-1}$ , n=12; p=0.028) in the Weddell Sea (Fig. S5). In contrast, ciliates showed  
 534 slightly higher abundances in the Weddell Sea, averaging  $4.5 \pm 8.2 \times 10^2$  cells  $L^{-1}$  (n=12) compared  
 535 to  $4.1 \pm 3.5 \times 10^1$  cells  $L^{-1}$  (n=7) in the Western Antarctic Peninsula.



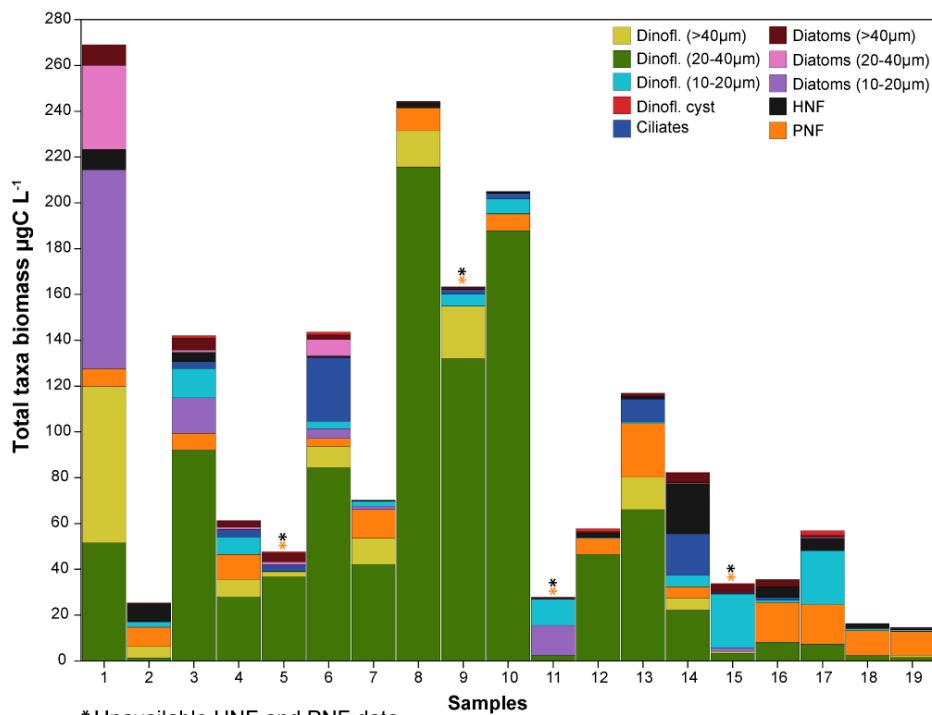


**Figure 3.** Biomass (µg C L<sup>-1</sup>) and proportions (represented by the ~~doughnut-charts~~barplots) of the main phytoplankton groups, protist and microzooplankton in the 19 samples obtained in the studied area (\*note that samples #5, #9, #11, #15 of HNF and PNF were lost).

### 3.3.6. Photosynthetic efficiency ( $F_v'/F_m'$ )

The ecophysiological state and fitness of phytoplankton ( $F_v'/F_m'$ ) ranged between 0.21 and 0.54, with an average of  $0.38 \pm 0.10$  (n=19). Values were slightly yet not significantly higher in the samples near the Antarctic Peninsula ( $0.41 \pm 0.06$ , n=7) compared to the samples collected in the Weddell Sea ( $0.36 \pm 0.11$ , n=12; p=0.36).

## 3.4 Chemical variables

### 3.4.1 Organic Carbon and Nitrogen



DOC and DON averaged  $62.5 \pm 32.5 \mu\text{M}$  (n=19) and  $6.1 \pm 3.1 \mu\text{M}$  (n=15), respectively, during this expedition (Table S5). Note that DON was below detection limit in ~~n=4~~ samples. Differences were observed between the two polar regions. Near the Antarctic Peninsula, DOC exhibited a lower concentration,  $57.6 \pm 7.4 \mu\text{M}$  (n=7), in contrast to the Weddell Sea, with slightly higher DOC levels ( $77.4 \pm 36.8 \mu\text{M}$ , n=12) (Table S5). Similarly, TN and DON concentrations were slightly higher in the Weddell Sea, measuring  $29.1 \pm 5.8 \mu\text{M}$  (n=12) and  $6.3 \pm 4.1 \mu\text{M}$  (n=10), respectively, compared to the Western Antarctic Peninsula, where concentrations of  $27.4 \pm 2.4 \mu\text{M}$  (n=7) and  $5.3 \pm 2.9 \mu\text{M}$  (n=5) were measured. The average contribution of dissolved amines (dMMA, dDMA, dTMA and dDEA) to DOC and DON was determined to be  $0.3 \pm 0.2 \%$  (n=19) and  $1.8 \pm 2.8 \%$  (n=15), respectively.

POC and PON were measured in all samples, with averages of  $7.6 \pm 5.3 \mu\text{M}$  (n=19) and  $1.2 \pm 0.9 \mu\text{M}$  (n=19), respectively (Table S5). Statistical analysis revealed significantly higher POC and PON concentrations in the Western Antarctic Peninsula (POC:  $10.7 \pm 7.3 \mu\text{M}$ , PON:  $1.8 \pm 1.2 \mu\text{M}$ , n = 7) than in the Weddell Sea (POC:  $5.7 \pm 1.7 \mu\text{M}$ , PON:  $0.9 \pm 0.2 \mu\text{M}$ , n = 12) (p=0.036 for POC and p=0.028 for PON) (Fig. S5). C:N ratio of POM closely approximated the canonical Redfield ratio of 6.6, with an observed mean of  $6.4 \pm 0.6$  (n=19) (Table S5). The contribution of particulate TMA to POC and PON averaged  $0.7 \pm 0.3 \%$  and  $1.5 \pm 0.6 \%$  (n=18 for both), respectively.

#### 3.4.2 Sulfur ~~Compounds~~compounds

DMSP concentrations averaged  $35.1 \pm 16.6 \text{ nM}$  considering all samples (n=19) (Table S5). A ~~small~~ disparity in the concentration of this sulfur compound was observed between the Western region of the Antarctic Peninsula and the Weddell Sea, where concentrations averaged  $44.8 \pm 20.9 \text{ nM}$  (n=7) and  $29.4 \pm 9.8 \text{ nM}$  (n=12), respectively. Similarly, DMS, the breakdown product of DMSP, showed statistically significant differences between samples, with higher values at the Western Antarctic Peninsula ( $1.7 \pm 0.4 \text{ nM}$ , n=7) and lower values in the Weddell Sea ( $1.0 \pm 0.4 \text{ nM}$ , n=12; p=0.011) (Table S5 and Fig. S5).

#### 3.4.3 Nutrients

Nutrient levels remained relatively stable throughout the duration of the cruise, with average concentrations of  $21.0 \pm 2.5$ ,  $0.2 \pm 0.0 \mu\text{M}$  for Nitrate, Nitrite, and  $54.9 \pm 6.1 \mu\text{M}$  for Silicate, respectively (n=19) (Table S5). Contrastingly, Ammonium, Phosphate and TP showed statistically

significant differences within the two marine areas with higher values for Weddell Sea,  $1.6 \pm 0.4$   $\mu\text{M}$  for Ammonium,  $2.3 \pm 0.2$   $\mu\text{M}$  for Phosphate and  $17.5 \pm 9.0$   $\mu\text{M}$  for TP compared to the Western Antarctic Peninsula area,  $0.8 \pm 0.2$  ( $n=19$ ;  $p<0.001$ ),  $1.9 \pm 0.3$  ( $n=19$ ;  $p=0.0098$ ) and  $4.9 \pm 1.9$   $\mu\text{M}$  ( $n=19$ ;  $p=0.0018$ ).

### 3.5 Multivariate statistical ~~Analysis~~analysis of the ~~Distributions~~distributions of Alkylamines, Microbiota, ~~Chemical~~alkylamines, microbiota, chemical and Environmental Variablesenvironmental variables

We investigated how seawater biogeochemistry influences amine concentrations to address the largely unexplored role of microbiology and ecology in marine alkylamine cycles. ~~A PCA analysis was~~Principal Component Analyses were conducted to examine correlations among a suite of physical, biogeochemical (including amine forms) variables and biomass data for microbial and viral populations of the 18 sampled stations (sample #3 was excluded because pTMA was missing) (Fig. 4). Variables like dMMA, DON, V4 and nanoflagellate biomasses were excluded from the PCA analyses because ~~several values they were below detection limit or missing~~not detected in all samples, dinoflagellates and diatoms 10–20  $\mu\text{m}$  biomass, TN, TOC and TON were excluded because they overlapped with included variables. Overall, the distribution of variable vectors within the multidimensional space of the PCA should help understand how environmental and biological variables influence the variability of marine alkylamines.

The first PCA ~~results~~, PCA (a), (Fig. 4a) provided an integrative perspective on the microbial community structure, encompassing the biomass of total bacteria, virus, phytoplankton biomasses (phytoplankton  $> 1$   $\mu\text{m}$ , including cryptophytes quantified by flow cytometry; and dinoflagellates cysts, dinoflagellates and diatoms  $>20$   $\mu\text{m}$  biomass, determined by optical microscopy) and biomass estimates for ciliates, assessed via optical microscopy. Additionally, it included physical (SST, salinity, PAR) and biogeochemical (DMSP, DMS, Chlorophyll-a,  $F_v'/F_m'$ , POC, PON, DOC, TP and nutrients) variables. The first two principal components (PC1 and PC2) accounted for 57.4 % and 14.9 % of the total variance, respectively. In PCA (a), while abiotic factors (SST, ammonium, phosphate), particulate organic matter (POC, PON) and total virus biomass were the most significant contributors to PC1, pTMA, dDMA, DMSP, Nitrate and Silicate contributed predominantly in a positive direction to the PC2 axis (Fig. 4a). The observed methylamines were neither aligned with physical parameters, nor with phytoplankton biomass or chlorophyll-a, which

may be regulated by e.g. iron (Fe) availability (not measured in this study). However, they more strongly covaried with nutrient concentrations, particularly silicate, and DMSP. Note that the expedition took place during a transitional period, after the peak of the ice melt and associated diatom blooms, alongside the initial stages of sea-ice formation.

Figure 4b further delves into the second analysis, PCA (b), focusing on specific biomass categories, including phytoplankton 1–2 µm, phytoplankton 2–20 µm (including containing cryptophytes), diatoms 20–40 µm and >40 µm, dinoflagellates 20–40 µm and >40 µm, V1, V2 and V3 viral fractions, and HNA and LNA bacteria, each of them characterized through optical microscopy or FCM. This detailed analysis provides nuanced insights into the interplay between microbial community dynamics and seawater biogeochemistry. The first and third principal components—Principal Components (PC1 and PC3, which were the components that explained the largest variance of the amines) account for 54.6 % and 8.0 % of the total variability variance, respectively. In summary, in PCA (b), pTMA and dDMA were aligned with nanophytoplankton (2–20 µm) which included cryptophytes (*Cryptomonas* spp.) and not with the biomass of larger phytoplankton (Fig. 4b).

Varimax rotation was applied to the factors extracted via Principal Axis Factoring to enhance interpretability by maximizing the variance of factor loadings, resulting in more distinct and interpretable patterns (Jolliffe, 2002) (Jolliffe, 2002) using the same variables as those applied in the PCAs. All key parameters, detailed in Table 1, were included in the analyses to support a robust interpretation of the principal components—Principal Components. Five factors were selected from the scree analysis, in sum explaining 69 % (Table 1a) and 71 % (Table 1b) of the total data variance, respectively. Table 1 presents the loadings of the variables on the five rotated factors, indicating the strength of correlation of each variable and its respective factor. Loadings (positive or negative) above 0.2 (or below -0.2) were considered significant. Finally, Pearson correlations for all pairs of variables are presented in Fig. S6. Overall, the Factor Analysis reinforced the exploration of the combined contribution of alkylamines and other variables to the total variance observed in the previous PCA analyses. pTMA showed larger positive loadings in Factor 2 of Table 1(a) (along with nutrients and DMSP) and Factor 3 of Table 1(b) (with nanophytoplankton and *Cryptomonas* spp. and slightly with the V1 virus population). This suggests that pTMA mostly occurred in the nanophytoplankton size fraction (<20 µm), that

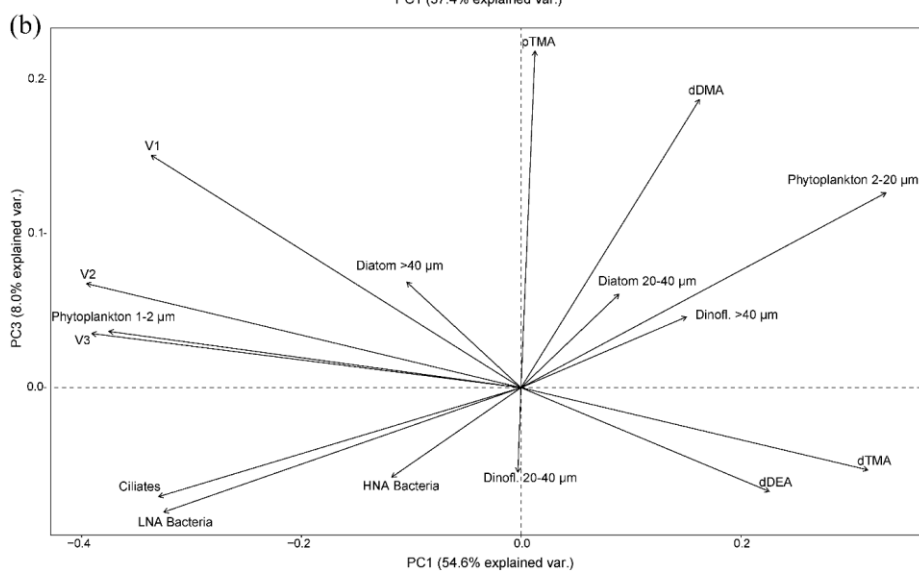
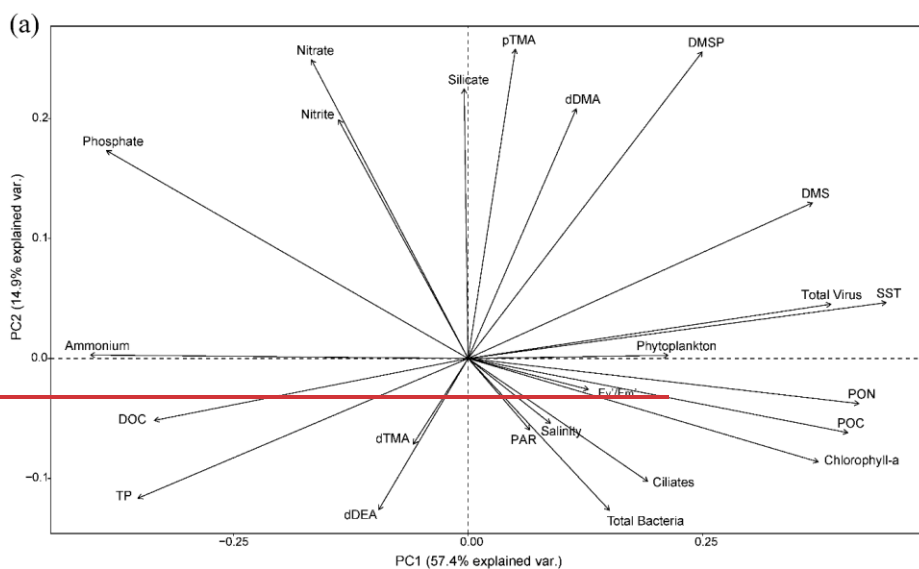
Formattato: SpazioPrima: 12 pt, Dopo: 10 pt

typically harbours most of the DMSP (Stefels et al., 2007). Also in the pairwise correlation analysis (Fig. S6), pTMA was best positively correlated with phytoplankton cells between 2 and 7  $\mu\text{m}$ , *Cryptomonas* spp. (Mantel statistical test  $r$  and p-value of 0.71 and 0.007, respectively), silicate (Mantel statistical test  $r$  and p-value of 0.63 and 0.01, respectively), as well as with DMSP (Mantel statistical test  $r$  and p-value of 0.51 and 0.034, respectively), PNF 10–20  $\mu\text{m}$  (Mantel statistical test  $r$  and p-value of 0.37 and 0.037, respectively), HNF and particularly HNF 2–5  $\mu\text{m}$  (Mantel statistical test  $r$  and p-value of 0.49 and 0.03, respectively). Conversely, it was negatively correlated with big diatoms (>40  $\mu\text{m}$ ) ( $p < 0.1$ ). Dissolved TMA showed its largest negative and positive loadings in Factor 1 and 3 of Table 1(a), together with chlorophyll-a and particulate organic matter, and Factor 1 and 4 of Table 1(b), where it was essentially correlated with nanophytoplankton. Indeed, in the correlation matrix (Fig. S6) dTMA correlated with phytoplankton cells between 7 and 15  $\mu\text{m}$  (Mantel statistical test  $r$  and p-value of 0.53 and 0.025, respectively), and more generally with phytoplankton cells ranging from 2 to 20  $\mu\text{m}$  (Mantel statistical test  $r$  and p-value of 0.45 and 0.004, respectively).

Dissolved DMA contributed significantly to Factor 2 in Table 1(a) and similarly in several Factors in Table 1(b), concurring with pTMA, DMSP, photosynthetic cells in the 2–20  $\mu\text{m}$  size range, HNA Bacteria, and nutrients (particularly silicate). In the correlation matrix (Fig. S6), dDMA was positively correlated with particulate TMA (Mantel statistical test  $r$  and p-value of 0.60 and 0.029, respectively), *Cryptomonas* spp. (Mantel statistical test  $r$  and p-value of 0.65 and 0.043, respectively), DMSP (Mantel statistical test  $r$  and p-value of 0.61 and 0.017, respectively), silicate (Mantel statistical test  $r$  and p-value of 0.72 and 0.004, respectively), nanoflagellate abundances, PNF (10–20  $\mu\text{m}$ ), HNF, and small HNF (2–5  $\mu\text{m}$ ) (Mantel statistical test  $r$  and p-value of 0.52 and 0.02, respectively).

Dissolved DEA had several similar positive and negative loadings in Table 1(a), which was also contributed by bacteria and general phytoplankton biomasses, and  $F_v'/F_m'$ . Additionally, dDEA contributed principally to Factor 5 in Table 1(b) together with HNA Bacteria. In pairwise correlations (Fig. S6), dDEA showed positive correlations with  $F_v'/F_m'$  (also indicated by the Mantel statistical test with  $r$  and p-value, 0.24 and, 0.038, respectively) and DMS (Mantel statistical test with  $r$  and p-value, 0.45, 0.046, respectively), and with dinoflagellate cysts, small dinoflagellates (10–20  $\mu\text{m}$ ) and big diatoms (>40  $\mu\text{m}$ ) ( $p < 0.1$ ).

668 Finally, dMMA, which was excluded from the PCA and Factor analysis as it was below detection  
669 limit in most cases, is known to originate primarily from the bacterial degradation of N-containing  
670 osmolytes and amino acids (Lidbury et al., 2015b; Mausz and Chen, 2019). dMMA exhibited a  
671 significant positive correlation with DOC (Mantel statistical test  $r$  and p-value of 0.49 and 0.016,  
672 respectively) and TOC (Mantel statistical test  $r$  and p-value of 0.48 and 0.02, respectively,) and  
673 negative correlation with total and HNA bacteria biomass (Mantel statistical test  $r$  and p-value of  
674 -0.28 and 0.04, respectively), salinity (Mantel statistical test  $r$  and p-value of -0.43 and 0.012,  
675 respectively), and SST (Fig. 5 and discussed in the following sections.



676

677 [S6](#).

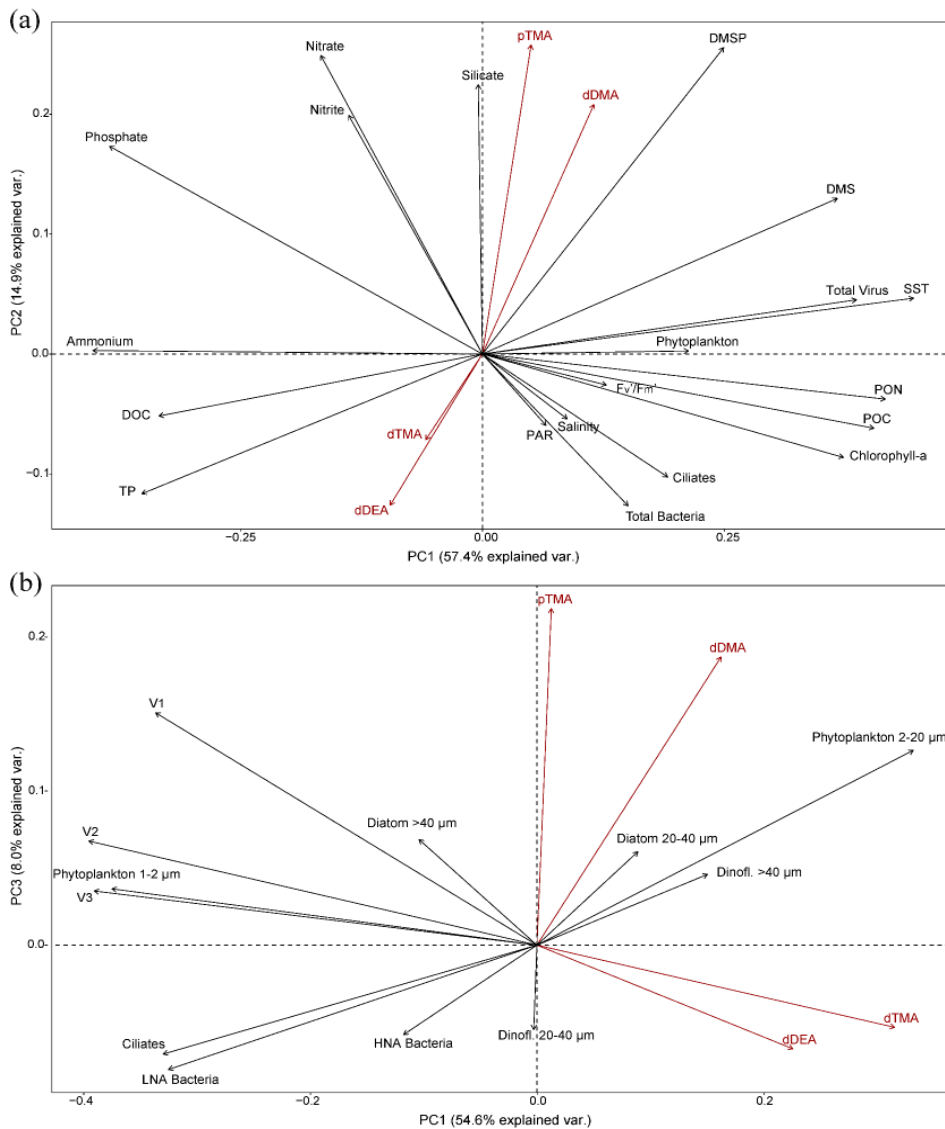


**Figure 4.** Principal component analyses of the biogeochemical-highest explanatory biogeochemical parameters in the 18 underway seawater samples collected (see text). (a) PC2 vs PC1; with of all physical and biogeochemical data from the water samples and the biomass of the main phytoplankton groupgroups and viral, bacterial and ciliate biomasses and (b) PC3 vs PC1; a of the more specific PCA withrun considering the biomasses of size-resolved

683 phytoplankton types and ciliates, active and non-active bacterial cells and the virus fractions. The percentage of  
684 explained variance is given on each principal component axis. *Amine forms are in red to facilitate visualization.*

685 **Table 1.** Factor ~~analysis~~*Analysis* loadings corresponding to the PCA analyses shown in Fig. 4, after  
686 Varimax rotation. The upper part of the Table, Variables (a) refers to PCA (a) (Fig. 4a), while the bottom  
687 part refers to PCA (b) (Fig. 4b). Loadings above 0.2 (or below -0.2) (significant loadings) are shown in  
688 ~~italics~~*italics*, and above 0.6 (or below -0.6) in **bold italics**. The last two lines of each table refer to the total  
689 variance explained by one factor in the data (SS Loadings) and to the proportion of the total variance in the  
690 dataset (Proportion Var.).

Variables (a)	Factor 1	Factor 2	Factor 3	Factor 4	Factor 5
pTMA	0.1	0.50	-0.21	0.03	0.30
dTMA	-0.40	-0.08	0.41	-0.14	0.00
dDMA	0.11	0.74	0.44	-0.07	0.09
dDEA	-0.25	0.01	0.39	0.32	-0.35
Chlorophyll-a	0.26	-0.10	<b>0.85</b>	0.10	0.31
SST	<b>0.92</b>	0.15	0.24	0.12	0.29
Salinity	0.03	0.09	0.20	<b>0.96</b>	-0.05
F <sub>v</sub> '/F <sub>m</sub> '	0.06	0.00	0.03	<b>0.72</b>	0.18
PAR	-0.07	0.13	0.51	0.26	-0.10
DMSP	0.10	0.58	0.25	-0.04	<b>0.68</b>
DMS	0.43	0.16	0.09	0.05	<b>0.70</b>
Total Bacteria	0.47	-0.10	0.12	0.41	-0.28
Total Virus	<b>0.87</b>	0.09	0.05	0.09	0.25
Phytoplankton	-0.17	-0.16	0.19	0.27	<b>0.74</b>
Ciliates	0.55	-0.28	-0.12	-0.05	0.02
Nitrate	-0.13	<b>0.69</b>	-0.35	0.16	0.01
Nitrite	-0.03	0.57	-0.11	-0.24	-0.09
Ammonium	<b>-0.80</b>	0.04	-0.25	0.05	-0.15
Silicate	-0.06	<b>0.91</b>	0.29	0.25	0.00
Phosphate	-0.51	0.55	-0.45	0.09	-0.22
DOC	-0.40	0.01	0.02	-0.48	-0.52
PON	0.39	-0.01	<b>0.74</b>	0.09	0.42
POC	0.35	-0.07	<b>0.74</b>	0.13	0.41
TP	-0.27	-0.03	-0.17	0.13	<b>-0.72</b>
SS Loadings	4.10	3.28	3.37	2.34	3.30



691[illegible]

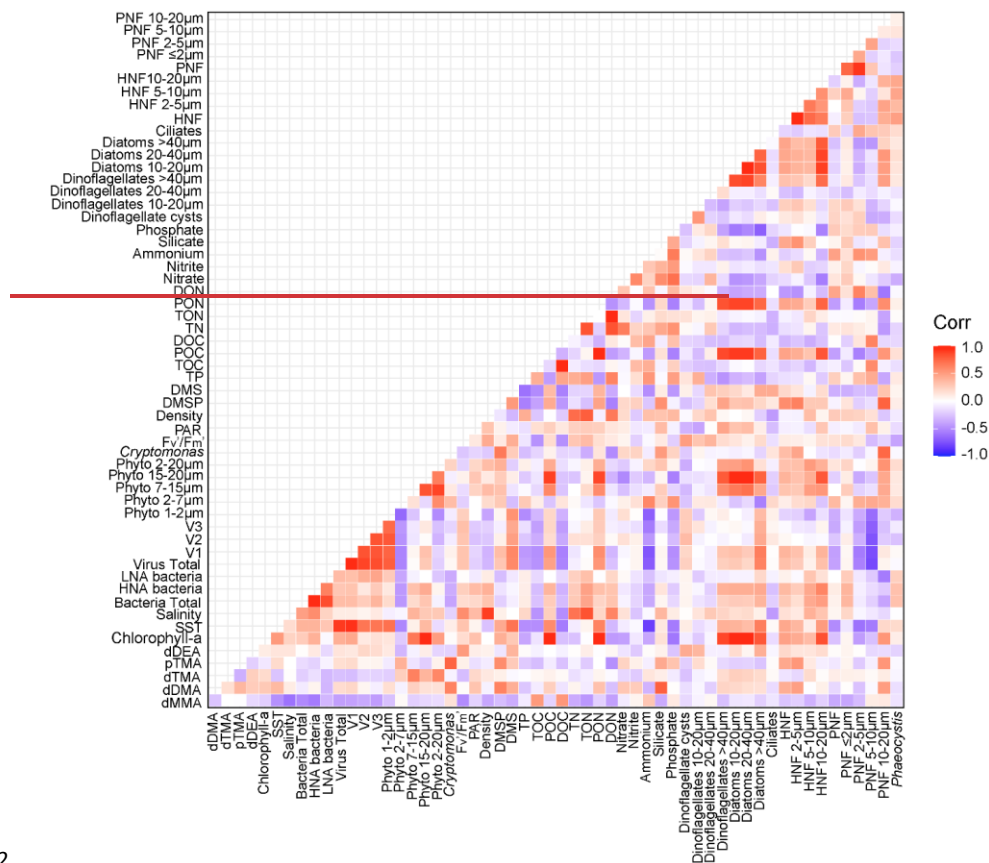


**Figure 5.** Heatmap showing Pearson's correlations between all the marine biogeochemical variables ("n" varied across parameters; details are provided in the Supplementary tables).

## 4 Discussion

### 4.1 Alkylamine distributions

The almost exclusive detection of TMA in particles suggests that this may be the predominant form of methylated amines within cells. It also Release from cells explains that dissolved TMA is consistently present in all our seawater samples, together with the fact that TMA has the lowest Henry's constant, indicating it is the most soluble amine. This tertiary amine is known to be the primary compound released during the decomposition of marine algae and microorganisms, marsh

grasses and fish, mainly as a breakdown product of quaternary amine precursors (Mausz and Chen, 2019; Sun et al., 2019). Three other dissolved (Mausz and Chen, 2019; Sun et al., 2019). Three other alkylamines were detected dissolved in seawater. Their distributions varied across regions around the Antarctic Peninsula: the samples off the Western Antarctic Peninsula harboured different total dissolved amine concentrations ( $78.3 \pm 44.7$  nM;  $n=7$ ) from those from the northern Weddell Sea ( $42.4 \pm 24.9$  nM;  $n=12$ ) (Fig. 2a). This coincided with slightly higher Chl-a levels west of the Antarctic Peninsula (Fig. 1, Table S2 and Fig. S5). Also,  $F_v'/F_m'$  values were slightly higher in samples from the Antarctic Peninsula, indicating greater photosynthetic efficiency and suggesting that in this area phytoplankton were in better physiological condition than in the Weddell Sea. Given the relatively minor differences in phytoplankton abundances and composition between the two areas, this difference can likely be attributed to higher iron (Fe) availability and light levels near the Antarctic Peninsula. The potential effect of light stress on the  $F_v'/F_m'$  cannot be ruled out, since waters of the Weddell Sea were clearer and more stratified (data not shown), hence more exposed to excess of damaging sunlight. Most samples were collected at 18:00 local time, which corresponds to daylight hours during the Austral summer. Potential diel variations in amine concentrations should be taken into account in future studies.

Regional differences also occurred. Amines have been measured in seawater in polar regions primarily by Gibb and Hatton (2004), who used a flow-diffusion gas chromatography method with selective nitrogen detection in Marguerite Bay, Antarctica, and by Dall'Osto et al. (2017, 2019), with subsequent methodological improvements introduced by Akenga and Fitzsimons (2024). Gibb and Hatton (2004) reported maximum dMMA concentrations of 36 nM, while Dall'Osto et al. (2017, 2019) observed concentrations of total methylated amines (3–10 nM) that were significantly lower than those measured in the present study. Here, we found regional differences in the composition of the alkylamine mixture. In the proximity to the Western Antarctic Peninsula, dMMA was absent, with dDMA dominating, contributing up to 64 % of the total dissolved amines, followed by dTMA with a 27 % contribution and dDEA with 9 % (Fig. 2a). Conversely, samples collected within the Weddell Sea exhibited a distinct composition, with TMA comprising the highest proportion at 50 %, followed by dDMA at 27 %, dDEA at 16 % and dMMA at 7 %. Alkylamines In this study, dDEA concentrations are similar to the range reported by van Pinxteren et al. (2019) for the SML and seawater in tropical waters (9 to 23 nM). Overall, alkylamines can

be released through various processes, including excretion by primary producers and bacterial activity, protist egestion, sloppy feeding by predators, and viral lysis (~~Bronk, 2002~~). ~~Phytoplankton and bacteria function as producers and consumers of DON (Antia et al., 1991; Bronk, 2002; Wheeler et al., 1974; Wheeler and Kirchman, 1986)~~(Bronk, 2002). This agrees with the fact that ~~phytoplankton and bacteria function as DON producers (Antia et al., 1991; Bronk, 2002; Wheeler et al., 1974; Wheeler and Kirchman, 1986)~~.

Phytoplankton release DON actively through mechanisms such as osmotic adjustments, reduced N excretion in response to changes in light, and autolysis. Phytoplanktonic passive release can occur due to physiological stress induced by factors such as ultraviolet radiation, temperature fluctuations, and light variations, as well as interactions with microzooplankton grazing and viral infections leading to lysis (~~Bronk, 2002~~).(Bronk, 2002). Viruses further contribute to DON production by inducing host cell lysis during the final stages of infection, releasing the cellular contents into the environment (~~Bronk, 2002~~).(Bronk, 2002). Similar processes are expected to occur with methylated amines (~~Sun et al., 2019~~).(Sun et al., 2019). Releasing N-rich dissolved organic matter (DOM) demands considerable energy from healthy phytoplankton cells (~~Ward and Bronk, 2001~~).(Ward and Bronk, 2001). In the Southern Ocean, N is generally not limiting because its use is limited by Fe and light; however, in the Western Antarctic Peninsula, where primary production can likely be supplied with Fe and other micronutrients from land, inorganic N may become depleted in phytoplankton blooms reaching limiting levels, as observed in ~~Dittrich et al. (2022)~~.Dittrich et al. (2022). Under these specific conditions, ~~phytoplankton can also act as DON consumers, and~~ the recycling of phytoplankton-released DON may provide an essential, bioavailable N source for sustaining phytoplankton growth. Notably, it has been reported that phytoplankton like the chlorophyte *Platymonas* (phototrophic nanoflagellate) incorporate primary amines from natural seawater efficiently, potentially supporting robust growth (~~North, 1975~~).(North, 1975). Similarly, diatoms have demonstrated efficient uptake of alkylamines (~~Wheeler and Hellebust, 1981~~)(Wheeler and Hellebust, 1981).

Bacteria are identified as the primary consumers and transformers of organic matter, as evidenced by the relationships between bacterial abundance and DON and DOC concentrations (Fig. 5S6). Furthermore, methylamine-degrading bacteria play a crucial role in releasing bioavailable N from alkylamines, which supports diatom growth, while diatoms provide organic C to bacteria in a

mutualistic exchange (Stein, 2017; Suleiman et al., 2016). (Stein, 2017; Suleiman et al., 2016). Moreover, marine bacteria metabolize methylamines as a N source via different pathways facilitating direct assimilation of N into biomass (Lidbury et al., 2015b; Sun et al., 2019; Taubert et al., 2017)(Lidbury et al., 2015b; Sun et al., 2019; Taubert et al., 2017). This recycling of amines may explain their nanomolar concentrations in seawater, suggesting they may serve as valuable organic N sources for both phytoplankton and bacteria. ~~The metabolism~~ Given their volatile nature, ~~alkylamines are also expected to be lost to the atmosphere. The cycle~~ of methylated amines shares several similarities with the cycles of methylated sulfur compounds, such as DMSP and DMS, in the marine environment. Both methylated amines and sulfur compounds originate from marine phytoplankton and participate in atmospheric processes. Recent studies have shown that TMA monooxygenase, an enzyme in marine bacteria, can oxidise both TMA and dimethylsulfide (Chen et al., 2011; Lidbury et al., 2016).(Chen et al., 2011; Lidbury et al., 2016). Thus, parallelisms between marine methylated amines and ~~dimethylsulfide~~ DMS metabolism underscores the importance of studying these molecules in tandem.

#### 4.2 Correlations between ~~Alkylamines, Chemical~~alkylamines, chemical and Environmental Variables~~environmental variables, and the Microbial Community~~microbial community

~~The distribution of variable vectors within the multidimensional space of the PCA should help understand how environmental and biological variables influence the variance of marine alkylamines. In PCA (a), while abiotic factors (SST, ammonium, phosphate), particulate organic matter. Using PCA, Factor Analysis, pairwise correlation analyses and statistical Mantel test, we found that TMA appears to be predominantly produced intracellularly by nanophytoplankton. Subsequently, it is~~ and total virus biomass were the most significant contributors to PC1, pTMA, dDMA, DMSP, Nitrate and Silicate contributed predominantly in a positive direction to the PC2 axis (Fig. 4a). The observed methylamines were neither aligned with physical parameters, nor with phytoplankton biomass or chlorophyll a, which may be regulated by Fe availability (not measured in this study). However, they more strongly covaried with nutrient concentrations, particularly silicate, and DMSP. This suggested that, during our study and in the sampled region, pTMA and dDMA were not associated with diatoms, which use and deplete silicate when supplied with Fe, but with non-silicate demanding phytoplankton. Note that the expedition took place during a transitional period, after the peak of the ice melt and associated diatom blooms, alongside the

Formattato: SpazioPrima: 12 pt, Dopo: 10 pt

initial stages of sea ice formation. In PCA (b), pTMA and dDMA were aligned with nanophytoplankton (2–20  $\mu\text{m}$ ) which included cryptophytes (*Cryptomonas* spp.) and not with the biomass of larger phytoplankton (Fig. 4b).

The factor analysis reinforced the exploration of the combined contribution of alkylamines and other variables to the total variance observed in the previous PCA analyses. pTMA showed larger positive loadings in factor 2 of Table 1(a) (along with nutrients and DMSP) and factor 3 of Table 1(b) (with nanophytoplankton and *Cryptomonas* spp. and slightly with the V1 virus population). This suggests that pTMA mostly occurred in nano-sized (<20  $\mu\text{m}$ ) phytoplankton, the same phytoplankton fraction that typically harbours most of the DMSP (Stefels et al., 2007). Also in the pairwise correlation analysis (Fig. 5), pTMA was best positively correlated with phytoplankton cells between 2 and 7  $\mu\text{m}$ , *Cryptomonas* spp. (Mantel statistical test  $r$  and  $p$  value of 0.71 and 0.007, respectively), silicate (Mantel statistical test  $r$  and  $p$  value of 0.63 and 0.01, respectively), as well as with DMSP (Mantel statistical test  $r$  and  $p$  value of 0.51 and 0.034, respectively), PNF 10–20  $\mu\text{m}$  (Mantel statistical test  $r$  and  $p$  value of 0.37 and 0.037, respectively), HNF and particularly HNF 2–5  $\mu\text{m}$  (Mantel statistical test  $r$  and  $p$  value of 0.49 and 0.03, respectively). Conversely, it was negatively correlated with big diatoms (>40  $\mu\text{m}$ ) ( $p < 0.1$ ).

Dissolved TMA showed its largest negative and positive loadings in factor 1 and 3 of Table 1(a), together with chlorophyll *a* and particulate organic matter, and factor 1 and 4 of Table 1(b), where it was essentially correlated with nanophytoplankton. Indeed, in the correlation matrix (Fig. 5) dTMA correlated with phytoplankton cells between 7 and 15  $\mu\text{m}$  (Mantel statistical test  $r$  and  $p$  value of 0.53 and 0.025, respectively), and more generally with phytoplankton cells ranging from 2 to 20  $\mu\text{m}$  (Mantel statistical test  $r$  and  $p$  value of 0.45 and 0.004, respectively). TMA appears to be intracellularly produced primarily by nanophytoplankton and subsequently released into the environment through cellular stress, mortality, or even by mechanical processes like filtration during sampling. This could explain the observed pairwise opposite correlation between particulate and dissolved TMA. The production of TMA is likely linked to the enzymatic activity of TMAO reductase (Mausz and Chen, 2019)(Mausz and Chen, 2019), an enzyme which, like dimethyl sulfoxide reductase (Spiese et al., 2009)(Spiese et al., 2009), occurs in marine bacteria but is potentially common in phytoplankton cells too. This enzyme reduces TMAO, a prevalent osmolyte like glycine betaine in phytoplankton (Gibb and Hatton, 2004).

Dissolved DMA contributed significantly to factor 2 in Table 1(a) and similarly in several factors (Gibb and Hatton, 2004). In Table 1(b), concurring with pTMA, DMSP, photosynthetic cells in the 2–20 µm size range, HNA Bacteria, and nutrients (particularly silicate). In the correlation matrix (Fig. 5), dDMA was positively correlated with particulate TMA (Mantel statistical test  $r$  and  $p$ -value of 0.60 and 0.029, respectively), *Cryptomonas* spp. (Mantel statistical test  $r$  and  $p$ -value of 0.65 and 0.043, respectively), DMSP (Mantel statistical test  $r$  and  $p$ -value of 0.61 and 0.017, respectively), silicate (Mantel statistical test  $r$  and  $p$ -value of 0.72 and 0.004, respectively), nanoflagellate abundances, PNF (10–20 µm), HNF, and small HNF (2–5 µm) (Mantel statistical test  $r$  and  $p$ -value of 0.52 and 0.02, respectively). Dissolved DMA appears to exhibit a causal relationship with particulate TMA, suggesting a shared phenomenology or a common origin. TheseThe statistical associations suggest that dDMA is linked to nanophytoplankton, potentially originating from the degradation of TMA or TMAO by bacteria or phytoplankton themselves. In aerobic conditions, DMA is produced from TMAO via TMAO demethylase (Barrett and Kwan, 1985; Lidbury et al., 2014)(Barrett and Kwan, 1985; Lidbury et al., 2014). Although there are no reports of TMAO demethylase activity has not yet been reported in phytoplankton cells, its presence in fish tissues (Kimura et al., 2000)(Kimura et al., 2000) suggests it could and the direct evidence of TMAO occurrence in polar diatoms (Dawson et al., 2020; Fitzsimons et al., 2024) suggest that this enzyme may also occur in eukaryotic microalgae too. Therefore, Although the involvement of a TMAO demethylation or any other enzyme requires genomic confirmation, our findings suggest that phytoplankton could directly release DMA or indirectly through bacteria attached to the outer membrane or residing in the phycosphere. In tropical waters, van Pinxteren et al. (2019)van Pinxteren et al. (2019) reported positive correlation between the pigment amines and pigments (fucoxanthin, and chlorophyll-a, and amines,) suggesting that amine production was fuelled by algal metabolism, most likely diatoms. In our study in polar waters, we found that TMA and dissolved DMA were closely related to nanosized phytoplankton.

Dissolved DEA had several similar positive and negative loadings in Table 1(a), which was also contributed by bacteria and general phytoplankton biomasses, and  $F_w^2/F_m^2$ . Additionally, dDEA contributed principally to factor 5 in Table 1(b) together with HNA Bacteria. In pairwise correlations (Fig. 5), dDEA showed positive correlations with  $F_w^2/F_m^2$  (also indicated by the Mantel statistical test with  $r$  and  $p$ -value, 0.24 and, 0.038, respectively) and DMS (Mantel

ha formattato: Colore carattere: Automatico

statistical test with  $r$  and  $p$ -value, 0.45, 0.046, respectively), and with dinoflagellate cysts, small dinoflagellates (10–20  $\mu\text{m}$ ) and big diatoms ( $>40 \mu\text{m}$ ) ( $p < 0.1$ ). Overall, dDEA exhibited an inverse correlation with particulate TMA. Notably, dDEA did not display a strong distributional alignment with any specific microbial variables, although a weak association with active bacteria was observed. Additionally, dDEA showed a moderate positive correlation with the photosynthetic efficiency of phytoplankton cells ( $F_v'/F_m'$ ) and with different phytoplankton groups compared to MAs. As expected,  $F_v'/F_m'$  displayed an inverse relationship to nutrient availability. As mentioned above, in the Southern Ocean,  $F_v'/F_m'$  declines when Feiron availability limits primary productivity despite the presence of elevated macronutrient concentrations (Wu et al., 2019)(Wu et al., 2019). Although the precise source of dDEA remains unclear, these findings demonstrate that DEA is widespread in Antarctic waters and follows distinct biological and biogeochemical pathways compared to MAs. We speculate that DEA may be formed by degradation of an amino acid precursor, potentially proline, considered an important N-bearing osmolyte (Fitzsimons et al., 2024)(Fitzsimons et al., 2024). However, further research is needed to identify its specific origins and the processes governing its distribution.

Finally, dMMA, which was excluded from the PCA and factor analysis as it was below detection limit in most cases, is known to originate primarily from the bacterial degradation of N-containing osmolytes and amino acids (Lidbury et al., 2015b; Mausz and Chen, 2019). Finally, regarding dMMA, the labile and volatile nature of this compound, dMMA exhibited a significant positive correlation with DOC (Mantel statistical test  $r$  and  $p$ -value of 0.49 and 0.016, respectively) and TOC (Mantel statistical test  $r$  and  $p$ -value of 0.48 and 0.02, respectively,) and negative correlation with total and HNA bacteria biomass (Mantel statistical test  $r$  and  $p$ -value of -0.28 and 0.04, respectively), salinity (Mantel statistical test  $r$  and  $p$ -value of -0.43 and 0.012, respectively), and SST (Fig. 5). This may suggest that bacteria efficiently remineralize dMMA into ammonium (Lidbury et al., 2015b), leading to the rapid depletion of MMA in the environment. Zhang et al. (2023)(Lidbury et al., 2015b), and that MMA volatilizes quickly to the atmosphere, both processes contributing to the rapid depletion of MMA in surface waters. Zhang et al. (2023) demonstrated that elevated salinity enhances the tendency of amines to volatilize from surface seawater by suppressing amine ionisation, thereby increasing exchange fluxes.



Altogether, the multivariate and pairwise correlation analyses make us concur with previous works in that phytoplankton are the primary producers of amines or amine precursors (~~Fitzsimons et al., 2023; van Pinxteren et al., 2019; Poste et al., 2014~~)(Fitzsimons et al., 2023; van Pinxteren et al., 2019; Poste et al., 2014). However, we identify nanophytoplankton and ~~smaller~~ *Cryptomonas* spp. populations, instead of diatoms, as the main responsible for TMA and DMA production in Antarctic waters in late summer. Smaller phytoplankton, likely those that are better adapted to thrive under iron-limited conditions, (Schoffman et al., 2016), would synthesise and harbour most of the intracellular TMA. Part of it would be released likely through processes such as cell mortality or through physiologically-driven DOM excretion. Likewise, DMA was statistically associated with small phytoplankton cells and heterotrophic nanoflagellates (PNF and HNF, respectively) as well as DMSP, exhibiting a distribution similar to the sulfur osmolyte. DMA was more closely associated with phytoplankton than with bacteria, which are expected to be responsible for TMA demethylation into DMA. This suggests that DMA is largely produced from phytoplankton TMA or TMAO by the algal cells themselves or closely associated bacteria. Finally, the distribution of DEA suggests distinct biogeochemical pathways compared to methylamines, potentially involving larger phytoplankton and bacterial communities. Notably, the factor most strongly linked to mortality, viruses, did not appear to influence alkylamine pathways. However, incorporating viral lysis as a key phenomenon in Antarctic phytoplankton dynamics is essential for advancing the understanding of microbial interactions and improving the accuracy of organic matter flux estimations in this climate-sensitive region (Biggs et al., 2021).

Our findings indicate that ~~alkylamines~~alkylamine distributions are ~~dependent on plankton~~linked to microplankton trophic webs, ~~with correlations to in~~ particular to certain phytoplankton cell ~~size~~size groups and ecophysiological conditions rather than to total biomass. Our approach does not allow us to quantify how much of the amines are produced directly by phytoplankton or through bacterial reworking of phytoplankton metabolites, yet we provide indications that both processes occur. Dissolved and particulate alkylamines accounted for non-negligible proportions of DON (ca. 1.8 %, with a maximum of 8.7 %), and of PON (ca. 1.5 %, with a maximum of 3.1 %). These proportions are reported here for the first time, providing a novel insight into the quantitative contribution of alkylamines to marine organic N pools.

Formattato: Tabulazioni: 0.8", Allineato a sinistra + Non a 2.08"

This study contributes to the necessity of increasing alkylamine determinations to be incorporated into future biogeochemical and climate models, given the pivotal role of alkylamines in both marine and atmospheric systems. In the Southern Ocean, biogenic emissions influence aerosol numbers through primary and secondary pathways, potentially enhancing CCN concentrations and modulating cloud albedo, thereby impacting regional radiative forcing (McCoy et al., 2015). Low-molecular-weight alkylamines contribute to both new particle formation (Brean et al., 2021) and aerosol growth, particularly in air masses passing over melting sea ice (Dall'Osto et al., 2017). Incorporating alkylamines in climate models for this climate-sensitive region requires gaining understanding of their distribution and drivers. The present study represents a step forward towards this aim.

## **5 Conclusion**

Alkylamines are seawater compounds whose role as precious organic nutrients in N transfer among trophic levels is starting to emerge. Despite their increasingly recognized importance, the distribution, biological sources, formation mechanisms, and emission strength of marine amines remain poorly known. This study provides several significant advances in the knowledge of the drivers of marine alkylamine concentrations and speciation. Overall, our results emphasise that alkylamines are embedded within marine microbial food webs, where phytoplankton, bacteria and viruses are interconnected, thereby influencing nutrient cycling, microbial dynamics, and the overall health of marine ecosystems. Our study, conducted under varying biogeochemical conditions, reveals that ~~methyamine~~~~stri-~~ and dimethylamine present in Antarctic surface waters were primarily sourced from ~~nano-sized-phytoplankton~~~~nanophytoplankton~~ cells and the associated bacteria and heterotrophic nanoflagellates, and diethylamine from hitherto unknown processes. Describing the distribution and ~~behaviour~~~~behavior~~ of alkylamines in the surface ocean is pivotal for understanding their roles in marine ~~ecosystems~~~~biogeochemical cycles~~, atmospheric chemistry, and climate.

ha formattato: Tipo di carattere: Non Grassetto

## **6 Author Contributions**

AR, MD'O, RS, and EB conceptualized and designed the study. AR and AS collected seawater and amine samples during the PolarChange Expedition. AR, under the supervision of MFF and

943 PA, processed and analyzed the amine samples, generating the amine dataset. MFF provided  
944 essential resources for the amine analysis. ELS, QG, MV, DV, CW, RS, and EB participated in  
945 the expedition, collected samples, and conducted biogeochemical and biological analyses. YMC  
946 and AR processed and analyzed flow cytometry samples at ICM. AR performed the statistical  
947 analyses, prepared the figures, and drafted the manuscript's first version. [AR](#), MFF, PA, CW, RS,  
948 and EB contributed to data interpretation and manuscript writing. All authors reviewed, revised,  
949 and approved the final version of the manuscript.

950

## 951 **7 Data availability**

952 All data are ~~shown~~[provided](#) in the Supplementary Information file.

953

## 954 **8 Competing Interests**

955 The authors declare that they have no conflict of interest.

956

## 957 **9 Acknowledgements**

958 We would like to thank the crew of the RV *Hesperides* for the logistic support, making possible  
959 the data collection of this study. Special thanks to Mara Abad and Núria González Fernández for  
960 TOC, TN and nutrient analyses at the Chemistry Service of the ICM-CSIC. We thank Jair Antonio  
961 Arévalo Lirio and Sofía Ibáñez Homedes for assistance counting flagellates and bacteria.

962

## 963 **10 Financial support**

964 AR was supported by the FPI grant (PRE2020-092994) from the Spanish Ministerio de Ciencia e  
965 Innovación (MICIN) and European Social Fund (ESF) ‘Investing in your Future’. The ~~POLAR~~  
966 ~~CHANGE~~[POLARCHANGE](#) project (PID2019-110288RB-I00) also received funding from the  
967 Spanish Ministerio de Ciencia e Innovación (MICIN). Further support was provided through an  
968 Advanced Grant from the European Research Council (ERC-2018-AdG #834162). This study is  
969 part of the POLARCSIC platform activities, and had the institutional support of the ‘Severo Ochoa  
970 Centre of Excellence’ accreditation (CEX2019-000928-S) to the ICM-CSIC.

971

972 **11 References**

973 Akenga, P. C. and Fitzsimons, M. F.: Automated method for the sensitive analysis of volatile  
974 amines in seawater, *ACS ES T Water*, 4, 2504–2510, [https://doi.org/Akenga, P. C. and Fitzsimons,  
975 M. F.: Automated method for the sensitive analysis of volatile amines in seawater, \*ACS ES T\*  
976 \*Water\*, 4, 2504–2510, <https://doi.org/10.1021/acsestwater.4c00007>, 2024.](https://doi.org/Akenga, P. C. and Fitzsimons, M. F.: Automated method for the sensitive analysis of volatile amines in seawater, ACS ES T Water, 4, 2504–2510, https://doi.org/10.1021/acsestwater.4c00007)

**Formattato:** SpazioDopo: 12 pt

**Codice campo modificato**

977 Álvarez-Salgado, X. A. and Miller, A. E. J.: Simultaneous determination of dissolved organic  
978 carbon and total dissolved nitrogen in seawater by high temperature catalytic oxidation: conditions  
979 for precise shipboard measurements, *Mar. Chem.*, 62, 325–333, [https://doi.org/Álvarez-Salgado,  
980 X. A. and Miller, A. E. J.: Simultaneous determination of dissolved organic carbon and total  
981 dissolved nitrogen in seawater by high temperature catalytic oxidation: conditions for precise  
982 shipboard measurements, \*Mar. Chem.\*, 62, 325–333, \[https://doi.org/10.1016/s0304-  
983 4203\\(98\\)00037-1\]\(https://doi.org/10.1016/s0304-4203\(98\)00037-1\), 1998.](https://doi.org/Álvarez-Salgado, X. A. and Miller, A. E. J.: Simultaneous determination of dissolved organic carbon and total dissolved nitrogen in seawater by high temperature catalytic oxidation: conditions for precise shipboard measurements, Mar. Chem., 62, 325–333, https://doi.org/10.1016/s0304-4203(98)00037-1)

**Codice campo modificato**

984 Antia, N. J., Harrison, P. J., and Oliveira, L.: The role of dissolved organic nitrogen in  
985 phytoplankton nutrition, cell biology and ecology, *Phycologia*, 30, 1–89, [https://doi.org/Antia, N.  
986 J., Harrison, P. J., and Oliveira, L.: The role of dissolved organic nitrogen in phytoplankton  
987 nutrition, cell biology and ecology, \*Phycologia\*, 30, 1–89, \[https://doi.org/10.2216/i0031-8884-30-  
988 1-1.1, 1991, 1991\]\(https://doi.org/10.2216/i0031-8884-30-1-1.1, 1991, 1991\).](https://doi.org/Antia, N. J., Harrison, P. J., and Oliveira, L.: The role of dissolved organic nitrogen in phytoplankton nutrition, cell biology and ecology, Phycologia, 30, 1–89, https://doi.org/10.2216/i0031-8884-30-1-1.1, 1991, 1991)

989 Auguie, B.: gridExtra: Miscellaneous Functions for "Grid" Graphics, Comprehensive R Archive  
990 Network (CRAN), 2017.

**Formattato:** SpazioPrima: 12 pt, Interlinea: multipla  
1.15 ri, Bordo: Superiore: (Nessun bordo), Inferiore:  
(Nessun bordo), A sinistra: (Nessun bordo), A destra:  
(Nessun bordo), Tra : (Nessun bordo)

**Codice campo modificato**

991 Barrett, E. L. and Kwan, H. S.: Bacterial reduction of trimethylamine oxide, *Annu. Rev.*  
992 *Microbiol.*, 39, 131–149, [https://doi.org/Barrett, E. L. and Kwan, H. S.: Bacterial reduction of  
993 trimethylamine oxide, \*Annu. Rev. Microbiol.\*, 39, 131–149,  
994 <https://doi.org/10.1146/annurev.mi.39.100185.001023>, 1985.](https://doi.org/Barrett, E. L. and Kwan, H. S.: Bacterial reduction of trimethylamine oxide, Annu. Rev. Microbiol., 39, 131–149, https://doi.org/10.1146/annurev.mi.39.100185.001023)

995 Biggs, T. E. G., Huisman, J., and Brussaard, C. P. D.: Viral lysis modifies seasonal phytoplankton  
996 dynamics and carbon flow in the Southern Ocean, *ISME J.*, 15, 3615–3622, [https://doi.org/Biggs,  
997 T. E. G., Huisman, J., and Brussaard, C. P. D.: Viral lysis modifies seasonal phytoplankton  
998 dynamics and carbon flow in the Southern Ocean, \*ISME J.\*, 15, 3615–3622,  
999 <https://doi.org/10.1038/s41396-021-01033-6>, 2021.](https://doi.org/Biggs, T. E. G., Huisman, J., and Brussaard, C. P. D.: Viral lysis modifies seasonal phytoplankton dynamics and carbon flow in the Southern Ocean, ISME J., 15, 3615–3622, https://doi.org/10.1038/s41396-021-01033-6)

**Codice campo modificato**

1000 Bolar, K.: STAT: Interactive Document for Working with Basic Statistical Analysis,  
1001 Comprehensive R Archive Network (CRAN), 2019.

**Formattato:** SpazioPrima: 12 pt, Interlinea: multipla  
1.15 ri, Bordo: Superiore: (Nessun bordo), Inferiore:  
(Nessun bordo), A sinistra: (Nessun bordo), A destra:  
(Nessun bordo), Tra : (Nessun bordo)

**Codice campo modificato**

1002 Brean, J., Dall'Osto, M., Simó, R., Shi, Z., Beddows, D. C. S., and Harrison, R. M.: Open ocean  
1003 and coastal new particle formation from sulfuric acid and amines around the Antarctic Peninsula,  
1004 *Nat. Geosci.*, 14, 383–388, [https://doi.org/Brean, J., Dall'Osto, M., Simó, R., Shi, Z., Beddows, D.  
1005 C. S., and Harrison, R. M.: Open ocean and coastal new particle formation from sulfuric acid and  
1006 amines around the Antarctic Peninsula, \*Nat. Geosci.\*, 14, 383–388,  
1007 <https://doi.org/10.1038/s41561-021-00751-y>, 2021.](https://doi.org/Brean, J., Dall'Osto, M., Simó, R., Shi, Z., Beddows, D. C. S., and Harrison, R. M.: Open ocean and coastal new particle formation from sulfuric acid and amines around the Antarctic Peninsula, Nat. Geosci., 14, 383–388, https://doi.org/10.1038/s41561-021-00751-y)

1008 Bronk, D. A.: Dynamics of DON, in: Biogeochemistry of Marine Dissolved Organic Matter,  
 1009 Elsevier, 153–247, <https://doi.org/Bronk, D. A.: Dynamics of DON, in: Biogeochemistry of>  
 1010 [https://doi.org/10.1016/b978-012323841-](https://doi.org/10.1016/b978-012323841-2/50007-5)  
 1011 [2/50007-5](https://doi.org/10.1016/b978-012323841-2/50007-5), 2002.

1012 Brussaard, C. P. D.: Optimization of procedures for counting viruses by flow cytometry, Appl.  
 1013 Environ. Microbiol., 70, 1506–1513, <https://doi.org/Brussaard, C. P. D.: Optimization of>  
 1014 [procedures for counting viruses by flow cytometry, Appl. Environ. Microbiol., 70, 1506–1513,](https://doi.org/10.1128/AEM.70.3.1506-1513.2004)  
 1015 <https://doi.org/10.1128/AEM.70.3.1506-1513.2004>, 2004.

1016 Brussaard, C. P. D., Thyrgaug, R., Marie, D., and Bratbak, G.: Flow cytometric analyses of viral  
 1017 infection in two marine phytoplankton species, Flow cytometric analyses of viral infection in two  
 1018 marine phytoplankton species, *Micromonas pusilla* (prasinophyceae) and *Phaeocystis pouchetii*  
 1019 (prymnesiophyceae), J. Phycol., 35, 941–948, [https://doi.org/-J. Phycol., 35, 941–948,](https://doi.org/-J. Phycol., 35, 941-948,)  
 1020 <https://doi.org/10.1046/j.1529-8817.1999.3550941.x>, 1999.

1021 Brussaard, C. P. D., Mari, X., Van Bleijswijk, J. D. L., and Veldhuis, M. J. W.: A mesocosm study  
 1022 of *Phaeocystis globosa* (Prymnesiophyceae) population dynamics, Harmful Algae, 4, 875–893,  
 1023 <https://doi.org/Brussaard, C. P. D., Mari, X., Van Bleijswijk, J. D. L., and Veldhuis, M. J. W.: A>  
 1024 [mesocosm study of \*Phaeocystis globosa\* \(Prymnesiophyceae\) population dynamics, Harmful](https://doi.org/10.1016/j.hal.2004.12.012)  
 1025 [Algae, 4, 875–893, https://doi.org/10.1016/j.hal.2004.12.012](https://doi.org/10.1016/j.hal.2004.12.012), 2005.

1026 Burg, M. B. and Ferraris, J. D.: Intracellular organic osmolytes: function and regulation, J. Biol.  
 1027 Chem., 283, 7309–7313, <https://doi.org/Burg, M. B. and Ferraris, J. D.: Intracellular organic>  
 1028 [osmolytes: function and regulation, J. Biol. Chem., 283, 7309–7313,](https://doi.org/10.1074/jbc.R700042200)  
 1029 <https://doi.org/10.1074/jbc.R700042200>, 2008.

1030 Chen, Y., Patel, N. A., Crombie, A., Scrivens, J. H., and Murrell, J. C.: Bacterial flavin-containing  
 1031 monooxygenase is trimethylamine monooxygenase, Proc. Natl. Acad. Sci. U. S. A., 108, 17791–  
 1032 17796, <https://doi.org/Chen, Y., Patel, N. A., Crombie, A., Scrivens, J. H., and Murrell, J. C.:>  
 1033 [Bacterial flavin-containing monooxygenase is trimethylamine monooxygenase, Proc. Natl. Acad.](https://doi.org/10.1073/pnas.1112928108)  
 1034 [Sci. U. S. A., 108, 17791–17796, https://doi.org/10.1073/pnas.1112928108](https://doi.org/10.1073/pnas.1112928108), 2011.

1035 Chistoserdova, L., Kalyuzhnaya, M. G., and Lidstrom, M. E.: The expanding world of  
 1036 methylotrophic metabolism, Annu. Rev. Microbiol., 63, 477–499, <https://doi.org/Chistoserdova,>  
 1037 [L., Kalyuzhnaya, M. G., and Lidstrom, M. E.: The expanding world of methylotrophic metabolism,](https://doi.org/10.1146/annurev.micro.091208.073600)  
 1038 [Annu. Rev. Microbiol., 63, 477–499, https://doi.org/10.1146/annurev.micro.091208.073600,](https://doi.org/10.1146/annurev.micro.091208.073600)  
 1039 2009.

1040 Corral, A. F., Choi, Y., Collister, B. L., Crosbie, E., Dadashazar, H., Digangi, J. P., Diskin, G.,  
 1041 Fenn, M. A., Kirschler, S., Moore, R., Nowak, J. B., Shook, M., Stahl, C., Shingler, T. J., Thornhill,  
 1042 K., Voigt, C., Ziemba, L., and Sorooshian, A.: Alkyl amines in cloud water: A case study over the  
 1043 northwest Atlantic ocean, Environ. Sci. Atmos., <https://doi.org/Corral, A. F., Choi, Y., Collister,>  
 1044 [B. L., Crosbie, E., Dadashazar, H., Digangi, J. P., Diskin, G., Fenn, M. A., Kirschler, S., Moore,](https://doi.org/10.1039/d2ea00117a)  
 1045 [R., Nowak, J. B., Shook, M., Stahl, C., Shingler, T. J., Thornhill, K., Voigt, C., Ziemba, L., and](https://doi.org/10.1039/d2ea00117a)  
 1046 [Sorooshian, A.: Alkyl amines in cloud water: A case study over the northwest Atlantic ocean,](https://doi.org/10.1039/d2ea00117a)  
 1047 [Environ. Sci. Atmos., https://doi.org/10.1039/d2ea00117a](https://doi.org/10.1039/d2ea00117a), 2022.

Codice campo modificato

Codice campo modificato

ha formattato: Colore carattere: Automatico

Formattato: SpazioPrima: 12 pt, Interlinea: multipla  
 1.15 ri, Bordo: Superiore: (Nessun bordo), Inferiore:  
 (Nessun bordo), A sinistra: (Nessun bordo), A destra:  
 (Nessun bordo), Tra : (Nessun bordo)

ha formattato: Colore carattere: Automatico

ha formattato: Colore carattere: Automatico

ha formattato: Colore carattere: Automatico

ha formattato: Colore carattere: Automatico

ha formattato: Colore carattere: Automatico

ha formattato: Colore carattere: Automatico

ha formattato: Colore carattere: Automatico

Codice campo modificato

Codice campo modificato

Codice campo modificato

Codice campo modificato

1048 Cree, C. H. L., Airs, R., Archer, S. D., and Fitzsimons, M. F.: Measurement of methylamines in  
 1049 seawater using solid phase microextraction and gas chromatography, *Limnol. Oceanogr. Methods*,  
 1050 **16**, 411–420, <https://doi.org/>, 2022.

1051 Cree, C. H. L., Airs, R., Archer, S. D., and Fitzsimons, M. F.: Measurement of methylamines in  
 1052 seawater using solid phase microextraction and gas chromatography, *Limnol. Oceanogr. Methods*,  
 1053 **16**, 411–420, <https://doi.org/10.1002/lom3.10255>, 2018.

1054 Dall'Osto, M., Ovadnevaite, J., Paglione, M., Beddows, D. C. S., Ceburnis, D., Cree, C., Cortés,  
 1055 P., Zamanillo, M., Nunes, S. O., Pérez, G. L., Ortega-Retuerta, E., Emelianov, M., Vaqué, D.,  
 1056 Marrasé, C., Estrada, M., Sala, M. M., Vidal, M., Fitzsimons, M. F., Beale, R., Airs, R., Rinaldi,  
 1057 M., Decesari, S., Cristina Facchini, M., Harrison, R. M., O'Dowd, C., and Simó, R.: Antarctic sea  
 1058 ice region as a source of biogenic organic nitrogen in aerosols, *Sci. Rep.*, **7**, 6047,  
 1059 <https://doi.org/>Dall'Osto, M., Ovadnevaite, J., Paglione, M., Beddows, D. C. S., Ceburnis, D.,  
 1060 Cree, C., Cortés, P., Zamanillo, M., Nunes, S. O., Pérez, G. L., Ortega-Retuerta, E., Emelianov,  
 1061 M., Vaqué, D., Marrasé, C., Estrada, M., Sala, M. M., Vidal, M., Fitzsimons, M. F., Beale, R.,  
 1062 Airs, R., Rinaldi, M., Decesari, S., Cristina Facchini, M., Harrison, R. M., O'Dowd, C., and Simó,  
 1063 R.: Antarctic sea ice region as a source of biogenic organic nitrogen in aerosols, *Sci. Rep.*, **7**, 6047,  
 1064 <https://doi.org/10.1038/s41598-017-06188-x>, 2017.

1065 Dall'Osto, M., Airs, R. L., Beale, R., Cree, C., Fitzsimons, M. F., Beddows, D., Harrison, R. M.,  
 1066 Ceburnis, D., O'Dowd, C., Rinaldi, M., Paglione, M., Nenes, A., Decesari, S., and Simó, R.:  
 1067 Simultaneous Detection of Alkylamines in the Surface Ocean and Atmosphere of the Antarctic  
 1068 Sympagic Environment, *ACS Earth Space Chem.*, **3**, 854–862, <https://doi.org/>, 2017.

1069 Dall'Osto, M., Airs, R. L., Beale, R., Cree, C., Fitzsimons, M. F., Beddows, D., Harrison, R. M.,  
 1070 Ceburnis, D., O'Dowd, C., Rinaldi, M., Paglione, M., Nenes, A., Decesari, S., and Simó, R.:  
 1071 Simultaneous Detection of Alkylamines in the Surface Ocean and Atmosphere of the Antarctic  
 1072 Sympagic Environment, *ACS Earth Space Chem.*, **3**, 854–862,  
 1073 <https://doi.org/10.1021/acsearthspacechem.9b00028>, 2019.

1074 Dittrich, R., Henley, S. F., Ducklow, H. W., and Meredith, M. P.: Dissolved organic carbon and  
 1075 nitrogen cycling along the west Antarctic Peninsula during summer, *Prog. Oceanogr.*, **206**,  
 1076 102854, <https://doi.org/>Dawson, H. M., Heal, K. R., Torstensson, A., Carlson, L. T., Ingalls, A.  
 1077 E., and Young, J. N.: Large diversity in nitrogen- and sulfur-containing compatible solute profiles  
 1078 in polar and temperate diatoms, *Integr. Comp. Biol.*, **60**, 1401–1413,  
 1079 <https://doi.org/10.1093/icb/icaa133>, 2020.

1080 Dittrich, R., Henley, S. F., Ducklow, H. W., and Meredith, M. P.: Dissolved organic carbon and  
 1081 nitrogen cycling along the west Antarctic Peninsula during summer, *Prog. Oceanogr.*, **206**,  
 1082 102854, <https://doi.org/10.1016/j.pocean.2022.102854>, 2022.

1083 Edler, L. and Elbrächter, M.: The Utermöhl method for quantitative phytoplankton analysis:  
 1084 Microscopic and molecular methods for quantitative phytoplankton analysis, 2010.

1085 Evans, C., Pearce, I., and Brussaard, C. P. D.: Viral-mediated lysis of microbes and carbon release  
 1086 in the sub-Antarctic and Polar Frontal zones of the Australian Southern Ocean, *Environ.*  
 1087 *Microbiol.*, **11**, 2924–2934, <https://doi.org/>Edler, L. and Elbrächter, M.: The Utermöhl method for

Codice campo modificato

Codice campo modificato

Codice campo modificato

quantitative phytoplankton analysis. Microscopic and molecular methods for quantitative phytoplankton analysis, 2010.

Evans, C., Pearce, I., and Brussaard, C. P. D.: Viral-mediated lysis of microbes and carbon release in the sub-Antarctic and Polar Frontal zones of the Australian Southern Ocean, *Environ. Microbiol.*, 11, 2924–2934, <https://doi.org/10.1111/j.1462-2920.2009.02050.x>, 2009.

Fitzsimons, M. F., Tilley, M., and Cree, C. H. L.: The determination of volatile amines in aquatic marine systems: A review, *Anal. Chim. Acta*, 1241, 340707, <https://doi.org/10.1016/j.aca.2022.340707>, 2023.

Fitzsimons, M. F., Tilley, M., and Cree, C. H. L.: The determination of volatile amines in aquatic marine systems: A review, *Anal. Chim. Acta*, 1241, 340707, <https://doi.org/10.1016/j.aca.2022.340707>, 2023.

Fitzsimons, M. F., Airs, R., and Chen, Y.: The occurrence and biogeochemical cycling of quaternary, ternary and volatile amines in marine systems, *Front. Mar. Sci.*, 11, <https://doi.org/10.3389/fmars.2024.1466221>, 2024.

Gasol, J. M. and Del Giorgio, P. A.: Using flow cytometry for counting natural planktonic bacteria and understanding the structure of planktonic bacterial communities, *Sci. Mar.*, 64, 197–224, <https://doi.org/10.3989/scimar.2000.64n2197>, 2000.

Gibb, S. W. and Hatton, A. D.: The occurrence and distribution of trimethylamine-N-oxide in Antarctic coastal waters, *Mar. Chem.*, 91, 65–75, <https://doi.org/10.1016/j.marchem.2004.04.005>, 2004.

Gibb, S. W., Mantoura, R. F. C., and Liss, P. S.: Ocean-atmosphere exchange and atmospheric speciation of ammonia and methylamines in the region of the NW Arabian Sea, *Global Biogeochem. Cycles*, 13, 161–178, <https://doi.org/10.1029/98gb00743>, 1999.

Goldwhite, H.: Nitrogen derivatives of the aliphatic hydrocarbons, in: *Rodd's Chemistry of Carbon Compounds*, Elsevier, 93–164, <https://doi.org/10.1016/b978-044453345-6.50475-2>, 1964.

Gorbunov, M. Y. and Falkowski, P. G.: Using chlorophyll fluorescence to determine the fate of photons absorbed by phytoplankton in the world's oceans, *Ann. Rev. Mar. Sci.*, 14, 213–238,

ha formattato: Colore carattere: Automatico

Codice campo modificato

Codice campo modificato

Codice campo modificato

Codice campo modificato

Codice campo modificato

Codice campo modificato

Codice campo modificato



1127 <https://doi.org/Gorbunov, M. Y. and Falkowski, P. G.: Using chlorophyll fluorescence to>  
1128 [determine the fate of photons absorbed by phytoplankton in the world's oceans, Ann. Rev. Mar.](https://doi.org/Gorbunov, M. Y. and Falkowski, P. G.: Using chlorophyll fluorescence to)  
1129 [Sci., 14, 213–238, https://doi.org/10.1146/annurev-marine-032621-122346](https://doi.org/10.1146/annurev-marine-032621-122346), 2022.

Codice campomodificato

1130 Gorbunov, M. Y., Shirsin, E., Nikonova, E., Fadeev, V. V., and Falkowski, P. G.: A multi-spectral  
1131 fluorescence induction and relaxation (FIRE) technique for physiological and taxonomic analysis  
1132 of phytoplankton communities, Mar. Ecol. Prog. Ser., 644, 1–13, <https://doi.org/Gorbunov, M. Y.,>  
1133 [Shirsin, E., Nikonova, E., Fadeev, V. V., and Falkowski, P. G.: A multi-spectral fluorescence](https://doi.org/Shirsin, E., Nikonova, E., Fadeev, V. V., and Falkowski, P. G.: A multi-spectral fluorescence)  
1134 [induction and relaxation \(FIRE\) technique for physiological and taxonomic analysis of](https://doi.org/Shirsin, E., Nikonova, E., Fadeev, V. V., and Falkowski, P. G.: A multi-spectral fluorescence)  
1135 [phytoplankton communities, Mar. Ecol. Prog. Ser., 644, 1–13, https://doi.org/10.3354/meps13358](https://doi.org/Shirsin, E., Nikonova, E., Fadeev, V. V., and Falkowski, P. G.: A multi-spectral fluorescence),  
1136 2020.

Codice campomodificato

1137 Grasshoff, K., Ehrhardt, M., and Kremling, K.: Methods of Seawater Analysis, 1983.

1138 Jakobsen, H. H. and Markager, S.: Carbon-to-chlorophyll ratio for phytoplankton in temperate  
1139 coastal waters: Seasonal patterns and relationship to nutrients, Limnol. Oceanogr., 61, 1853–1868,  
1140 <https://doi.org/Grasshoff, K., Ehrhardt, M., and Kremling, K.: Methods of Seawater Analysis,>  
1141 [1983.](https://doi.org/Grasshoff, K., Ehrhardt, M., and Kremling, K.: Methods of Seawater Analysis,)

1142 Jakobsen, H. H. and Markager, S.: Carbon-to-chlorophyll ratio for phytoplankton in temperate  
1143 coastal waters: Seasonal patterns and relationship to nutrients, Limnol. Oceanogr., 61, 1853–1868,  
1144 <https://doi.org/10.1002/lno.10338>, 2016.

Codice campomodificato

1145 Jolliffe, I. T.: Principal component analysis for special types of data, in: Principal Component  
1146 Analysis, Springer, New York, NY, 338–372, <https://doi.org/Jolliffe, I. T.: Principal component>  
1147 [analysis for special types of data, in: Principal Component Analysis, Springer, New York, NY,](https://doi.org/Jolliffe, I. T.: Principal component)  
1148 [338–372, https://doi.org/10.1007/0-387-22440-8\\_13](https://doi.org/10.1007/0-387-22440-8_13), 2002., 2002.

1149 Kassambara, A.: ggcorrplot: Visualization of a Correlation Matrix Using “ggplot2”,  
1150 Comprehensive R Archive Network (CRAN), 2021.

**Formattato:** SpazioPrima: 12 pt, Interlinea: multipla 1.15 ri, Bordo: Superiore: (Nessun bordo), Inferiore: (Nessun bordo), A sinistra: (Nessun bordo), A destra: (Nessun bordo), Tra : (Nessun bordo)

1151 Kassambara, A. and Mundt, F.: factoextra: Extract and Visualize the Results of Multivariate Data  
1152 Analyses, Comprehensive R Archive Network (CRAN), 2020.

**ha formattato:** Colore carattere: Automatico

1153 Kimura, M., Seki, N., and Kimura, I.: Occurrence and some properties of trimethylamine-N-oxide  
1154 demethylase in myofibrillar fraction from walleye pollack muscle, Fish. Sci., 66, 725–729,  
1155 <https://doi.org/Kimura, M., Seki, N., and Kimura, I.: Occurrence and some properties of>  
1156 [trimethylamine-N-oxide demethylase in myofibrillar fraction from walleye pollack muscle, Fish.](https://doi.org/Kimura, M., Seki, N., and Kimura, I.: Occurrence and some properties of)  
1157 [Sci., 66, 725–729, https://doi.org/10.1046/j.1444-2906.2000.00118.x](https://doi.org/10.1046/j.1444-2906.2000.00118.x), 2000.

Codice campomodificato

1158 Kinsey, J. D. and Kieber, D. J.: Microwave preservation method for DMSP, DMSO, and acrylate  
1159 in unfiltered seawater and phytoplankton culture samples: Microwave Sample Preservation  
1160 Method, Limnol. Oceanogr. Methods, 14, 196–209, <https://doi.org/Kinsey, J. D. and Kieber, D. J.:>  
1161 [Microwave preservation method for DMSP, DMSO, and acrylate in unfiltered seawater and](https://doi.org/Kinsey, J. D. and Kieber, D. J.:)  
1162 [phytoplankton culture samples: Microwave Sample Preservation Method, Limnol. Oceanogr.](https://doi.org/Kinsey, J. D. and Kieber, D. J.:)  
1163 [Methods, 14, 196–209, https://doi.org/10.1002/lom3.10081](https://doi.org/10.1002/lom3.10081), 2016.

Codice campomodificato



1164 Koester, I., Quinlan, Z. A., Nothias, L. F., White, M. E., Rabines, A., Petras, D., Brunson, J. K.,  
 1165 Dührkop, K., Ludwig, M., Böcker, S., Azam, F., Allen, A. E., Dorrestein, P. C., and Aluwihare,  
 1166 L. I.: Illuminating the dark metabolome of *Pseudo-nitzschia* microbiome associations, *Environ.*  
 1167 *Microbiol.*, 24, 5408–5424, <https://doi.org/10.1111/1462-2920.16242>, 2022.

1168 Landa, M., Burns, A. S., Roth, S. J., and Moran, M. A.: Bacterial transcriptome remodeling during  
 1169 sequential co-culture with a marine dinoflagellate and diatom, *ISME J.*, 11, 2677–2690,  
 1170 [https://doi.org/Koester, I., Quinlan, Z. A., Nothias, L.-F., White, M. E., Rabines, A., Petras, D.,  
 1171 Brunson, J. K., Dührkop, K., Ludwig, M., Böcker, S., Azam, F., Allen, A. E., Dorrestein, P. C.,  
 1172 and Aluwihare, L. I.: Illuminating the dark metabolome of Pseudo-nitzschia-microbiome  
 1173 associations, \*Environ. Microbiol.\*, 24, 5408–5424, <https://doi.org/10.1111/1462-2920.16242>,  
 1174 2022.](https://doi.org/Koester, I., Quinlan, Z. A., Nothias, L.-F., White, M. E., Rabines, A., Petras, D., Brunson, J. K., Dührkop, K., Ludwig, M., Böcker, S., Azam, F., Allen, A. E., Dorrestein, P. C., and Aluwihare, L. I.: Illuminating the dark metabolome of Pseudo-nitzschia-microbiome associations, Environ. Microbiol., 24, 5408–5424, https://doi.org/10.1111/1462-2920.16242, 2022.)

1175 Landa, M., Burns, A. S., Roth, S. J., and Moran, M. A.: Bacterial transcriptome remodeling during  
 1176 sequential co-culture with a marine dinoflagellate and diatom, *ISME J.*, 11, 2677–2690,  
 1177 <https://doi.org/10.1038/ismej.2017.117>, 2017.

1178 Lidbury, I., Murrell, J. C., and Chen, Y.: Trimethylamine N-oxide metabolism by abundant marine  
 1179 heterotrophic bacteria, *Proc. Natl. Acad. Sci. U. S. A.*, 111, 2710–2715, [https://doi.org/Lidbury,  
 1180 I., Murrell, J. C., and Chen, Y.: Trimethylamine N-oxide metabolism by abundant marine  
 1181 heterotrophic bacteria, \*Proc. Natl. Acad. Sci. U. S. A.\*, 111, 2710–2715,  
 1182 <https://doi.org/10.1073/pnas.1317834111>, 2014.](https://doi.org/Lidbury, I., Murrell, J. C., and Chen, Y.: Trimethylamine N-oxide metabolism by abundant marine heterotrophic bacteria, Proc. Natl. Acad. Sci. U. S. A., 111, 2710–2715, https://doi.org/10.1073/pnas.1317834111, 2014.)

1183 Lidbury, I., Kimberley, G., Scanlan, D. J., Murrell, J. C., and Chen, Y.: Comparative genomics  
 1184 and mutagenesis analyses of choline metabolism in the marine *Roseobacter* clade, *Environ.*  
 1185 *Microbiol.*, 17, 5048–5062, [https://doi.org/Lidbury, I., Kimberley, G., Scanlan, D. J., Murrell, J.  
 1186 C., and Chen, Y.: Comparative genomics and mutagenesis analyses of choline metabolism in the  
 1187 marine \*Roseobacter\* clade, \*Environ. Microbiol.\*, 17, 5048–5062, <https://doi.org/10.1111/1462-2920.12943>,  
 1188 2015a.](https://doi.org/Lidbury, I., Kimberley, G., Scanlan, D. J., Murrell, J. C., and Chen, Y.: Comparative genomics and mutagenesis analyses of choline metabolism in the marine Roseobacter clade, Environ. Microbiol., 17, 5048–5062, https://doi.org/10.1111/1462-2920.12943, 2015a.)

1189 Lidbury, I., Kröber, E., Zhang, Z., Zhu, Y., Murrell, J. C., Chen, Y., and Schäfer, H.: A mechanism  
 1190 for bacterial transformation of dimethylsulfide to dimethylsulfoxide: a missing link in the marine  
 1191 organic sulfur cycle, *Environ. Microbiol.*, 18, 2754–2766, [https://doi.org/Lidbury, I., Kröber, E.,  
 1192 Zhang, Z., Zhu, Y., Murrell, J. C., Chen, Y., and Schäfer, H.: A mechanism for bacterial  
 1193 transformation of dimethylsulfide to dimethylsulfoxide: a missing link in the marine organic sulfur  
 1194 cycle, \*Environ. Microbiol.\*, 18, 2754–2766, <https://doi.org/10.1111/1462-2920.13354>, 2016.](https://doi.org/Lidbury, I., Kröber, E., Zhang, Z., Zhu, Y., Murrell, J. C., Chen, Y., and Schäfer, H.: A mechanism for bacterial transformation of dimethylsulfide to dimethylsulfoxide: a missing link in the marine organic sulfur cycle, Environ. Microbiol., 18, 2754–2766, https://doi.org/10.1111/1462-2920.13354, 2016.)

1195 Lidbury, I. D. E. A., Murrell, J. C., and Chen, Y.: Trimethylamine and trimethylamine N-oxide  
 1196 are supplementary energy sources for a marine heterotrophic bacterium: implications for marine  
 1197 carbon and nitrogen cycling, *ISME J.*, 9, 760–769, [https://doi.org/Lidbury, I. D. E. A., Murrell, J.  
 1198 C., and Chen, Y.: Trimethylamine and trimethylamine N-oxide are supplementary energy sources  
 1199 for a marine heterotrophic bacterium: implications for marine carbon and nitrogen cycling, \*ISME\*  
 1200 \*J.\*, 9, 760–769, <https://doi.org/10.1038/ismej.2014.149>, 2015b.](https://doi.org/Lidbury, I. D. E. A., Murrell, J. C., and Chen, Y.: Trimethylamine and trimethylamine N-oxide are supplementary energy sources for a marine heterotrophic bacterium: implications for marine carbon and nitrogen cycling, ISME J., 9, 760–769, https://doi.org/10.1038/ismej.2014.149, 2015b.)

1201 Liu, C., Li, H., Zheng, H., Wang, G., Qin, X., Chen, J., Zhou, S., Lu, D., Liang, G., Song, X.,  
 1202 Duan, Y., Liu, J., Huang, K., and Deng, C.: Ocean emission pathway and secondary formation  
 1203 mechanism of aminiums over the Chinese marginal sea, *J. Geophys. Res.*, 127, <https://doi.org/Liu>,

Codice campo modificato

Codice campo modificato

Codice campo modificato

Codice campo modificato

Codice campo modificato

1204 C., Li, H., Zheng, H., Wang, G., Qin, X., Chen, J., Zhou, S., Lu, D., Liang, G., Song, X., Duan,  
1205 Y., Liu, J., Huang, K., and Deng, C.: Ocean emission pathway and secondary formation  
1206 mechanism of aminiums over the Chinese marginal sea, *J. Geophys. Res.*, 127,  
1207 <https://doi.org/10.1029/2022jd037805>, 2022.

Codice campo modificato

1208 Masdeu-Navarro, M., Mangot, J. F., Xue, L., Cabrera-Brufau, M., Gardner, S. G., Kieber, D. J.,  
1209 González, J. M., and Simó, R.: Spatial and diel patterns of volatile organic compounds, DMSP-  
1210 derived compounds, and planktonic microorganisms around a tropical scleractinian coral colony,  
1211 *Front. Mar. Sci.*, 9, <https://doi.org/10.3389/fmars.2022.944141>, 2022.  
1212 Marie, D., Rigaut-Jalabert, F., and Vaultot, D.: An improved  
1213 protocol for flow cytometry analysis of phytoplankton cultures and natural samples: AnImproved  
1214 Protocol for Flow Cytometry Analysis, *Cytometry A*, 85, 962–968,  
<https://doi.org/10.1002/cyto.a.22517>, 2014.

1215 Masdeu-Navarro, M., Mangot, J.-F., Xue, L., Cabrera-Brufau, M., Gardner, S. G., Kieber, D. J.,  
1216 González, J. M., and Simó, R.: Spatial and diel patterns of volatile organic compounds, DMSP-  
1217 derived compounds, and planktonic microorganisms around a tropical scleractinian coral colony,  
1218 *Front. Mar. Sci.*, 9, <https://doi.org/10.3389/fmars.2022.944141>, 2022.

Codice campo modificato

1219 Mausz, M. A. and Chen, Y.: Microbiology and ecology of methylated Amine metabolism in  
1220 marine ecosystems, *Curr. Issues Mol. Biol.*, 33, 133–148, <https://doi.org/10.21775/cimb.033.133>, 2019.  
1221 Mausz, M. A. and Chen, Y.: Microbiology and ecology of methylated Amine metabolism in marine ecosystems, *Curr.*  
1222 *Issues Mol. Biol.*, 33, 133–148, <https://doi.org/10.21775/cimb.033.133>, 2019.

Codice campo modificato

1223 Menden-Deuer, S. and Lessard, E. J.: Carbon to volume relationships for dinoflagellates, diatoms,  
1224 and other protist plankton, *Limnol. Oceanogr.*, 45, 569–579, <https://doi.org/10.1126/sciadv.1500157>, 2015.  
1225 McCoy, D. T., Burrows, S. M., Wood, R., Grosvenor, D. P., Elliott, S. M., Ma, P.-L., Rasch, P. J., and Hartmann,  
1226 D. L.: Natural aerosols explain seasonal and spatial patterns of Southern Ocean cloud albedo, *Sci.*  
1227 *Adv.*, 1, e1500157, <https://doi.org/10.1126/sciadv.1500157>, 2015.

1228 Menden-Deuer, S. and Lessard, E. J.: Carbon to volume relationships for dinoflagellates, diatoms,  
1229 and other protist plankton, *Limnol. Oceanogr.*, 45, 569–579,  
1230 <https://doi.org/10.4319/lo.2000.45.3.0569>, 2000.

Codice campo modificato

1231 Ning, A., Liu, L., Zhang, S., Yu, F., Du, L., Ge, M., and Zhang, X.: The critical role of  
1232 dimethylamine in the rapid formation of iodic acid particles in marine areas, *Npj Clim. Atmos.*  
1233 *Sci.*, 5, <https://doi.org/10.1038/s41612-022-00316-9>, 2022., 2022.  
1234 Ning, A., Liu, L., Zhang, S., Yu, F., Du, L., Ge, M., and Zhang, X.: The  
1235 critical role of dimethylamine in the rapid formation of iodic acid particles in marine areas, *Npj*  
*Clim. Atmos. Sci.*, 5, <https://doi.org/10.1038/s41612-022-00316-9>, 2022., 2022.

1236 Norland, S.: The relationship between biomass and volume of bacteria. In: *Handbook of Methods*  
1237 *in Aquatic Microbial Ecology*, edited by P. Kemp, B. Sherr, E. Sherr, and J. Cole, Lewis  
1238 Publishers, 1993.

**Formattato:** SpazioPrima: 12 pt, Interlinea: multipla  
1.15 ri, Bordo: Superiore: (Nessun bordo), Inferiore:  
(Nessun bordo), A sinistra: (Nessun bordo), A destra:  
(Nessun bordo), Tra : (Nessun bordo)

1239 North, B. B.: Primary amines in California coastal waters: Utilization by phytoplankton 1,  
1240 *Limnology and Oceanography*, 20, 20–27, 1975; North, B. B.: Primary amines in California coastal  
1241 waters: Utilization by phytoplankton 1, *Limnology and Oceanography*, 20, 20–27, 1975.

**ha formattato:** Colore carattere: Automatico

1242 Oksanen, J.: vegan: Community Ecology Package, Comprehensive R Archive Network (CRAN),  
1243 2022.

1244 Palenik, B. and Morel, F. M.: Amine oxidases of marine phytoplankton, *Appl. Environ. Microbiol.*,  
1245 57, 2440–2443, <https://doi.org/Palenik, B. and Morel, F. M.: Amine oxidases of marine phytoplankton, Appl. Environ. Microbiol., 57, 2440–2443, https://doi.org/10.1128/aem.57.8.2440-2443.1991>, 1991.

1248 van Pinxteren, M., Fomba, K. W., van Pinxteren, D., Triesch, N., Hoffmann, E. H., Cree, C. H. L.,  
1249 Fitzsimons, M. F., von Tümpling, W., and Herrmann, H.: Aliphatic amines at the Cape Verde  
1250 Atmospheric Observatory: Abundance, origins and sea air fluxes, *Atmos. Environ.* (1994), 203,  
1251 183–195, [https://doi.org/van Pinxteren, M., Müller, C., Iinuma, Y., Stolle, C., and Herrmann, H.: Chemical characterization of dissolved organic compounds from coastal sea surface microlayers \(Baltic Sea, Germany\), Environ. Sci. Technol., 46\(19\), 10455–10462, https://doi.org/10.1021/es204492b](https://doi.org/van Pinxteren, M., Müller, C., Iinuma, Y., Stolle, C., and Herrmann, H.: Chemical characterization of dissolved organic compounds from coastal sea surface microlayers (Baltic Sea, Germany), Environ. Sci. Technol., 46(19), 10455–10462, https://doi.org/10.1021/es204492b), 2012.

1255 van Pinxteren, M., Fomba, K. W., van Pinxteren, D., Triesch, N., Hoffmann, E. H., Cree, C. H. L.,  
1256 Fitzsimons, M. F., von Tümpling, W., and Herrmann, H.: Aliphatic amines at the Cape Verde  
1257 Atmospheric Observatory: Abundance, origins and sea-air fluxes, *Atmos. Environ.* (1994), 203,  
1258 183–195, <https://doi.org/10.1016/j.atmosenv.2019.02.011>, 2019.

1259 Poste, A. E., Grung, M., and Wright, R. F.: Amines and amine-related compounds in surface  
1260 waters: a review of sources, concentrations and aquatic toxicity, *Sci. Total Environ.*, 481, 274–  
1261 279, <https://doi.org/Poste, A. E., Grung, M., and Wright, R. F.: Amines and amine-related compounds in surface waters: a review of sources, concentrations and aquatic toxicity, Sci. Total Environ., 481, 274–279, https://doi.org/10.1016/j.scitotenv.2014.02.066>, 2014.

1264 Revelle, W.: psych: Procedures for Psychological, Psychometric, and Personality Research,  
1265 Comprehensive R Archive Network (CRAN), 2023.

1266 Rinaldi, M., Paglione, M., Decesari, S., Harrison, R. M., Beddows, D. C. S., Ovadnevaite, J.,  
1267 Ceburnis, D., O'Dowd, C. D., Simó, R., and Dall'Osto, M.: Contribution of Water-Soluble Organic  
1268 Matter from Multiple Marine Geographic Eco-Regions to Aerosols around Antarctica, *Environ.*  
1269 *Sci. Technol.*, 54, 7807–7817, <https://doi.org/Rinaldi, M., Paglione, M., Decesari, S., Harrison, R. M., Beddows, D. C. S., Ovadnevaite, J., Ceburnis, D., O'Dowd, C. D., Simó, R., and Dall'Osto, M.: Contribution of Water-Soluble Organic Matter from Multiple Marine Geographic Eco-Regions to Aerosols around Antarctica, Environ. Sci. Technol., 54, 7807–7817, https://doi.org/10.1021/acs.est.0c00695>, 2020.

1274 Rocchi, A., Sotomayor-Garcia, A., Cabrera-Brufau, M., Berdalet, E., Dall'Osto, M., and Vaque,  
1275 D.: Abundance and activity of sympagic viruses near the Western Antarctic Peninsula, *Polar Biol.*,  
1276 45, 1363–1378, <https://doi.org/Rocchi, A., Sotomayor-Garcia, A., Cabrera-Brufau, M., Berdalet, E., Dall'Osto, M., and Vaque, D.: Abundance and activity of sympagic viruses near the Western Antarctic Peninsula, Polar Biol., 45, 1363–1378, https://doi.org/10.1007/s00300-022-03073-w>,  
1278 2022.

1280 Sieracki, M. E., Johnson, P. W., and Sieburth, J. M.: Detection, enumeration, and sizing of

**Formattato:** SpazioPrima: 12 pt, Interlinea: multipla 1.15 ri, Bordo: Superiore: (Nessun bordo), Inferiore: (Nessun bordo), A sinistra: (Nessun bordo), A destra: (Nessun bordo), Tra : (Nessun bordo)

**ha formattato:** Colore carattere: Automatico

**Codice campo modificato**

**Codice campo modificato**

**Codice campo modificato**

**Formattato:** SpazioPrima: 12 pt, Interlinea: multipla 1.15 ri, Bordo: Superiore: (Nessun bordo), Inferiore: (Nessun bordo), A sinistra: (Nessun bordo), A destra: (Nessun bordo), Tra : (Nessun bordo)

**ha formattato:** Colore carattere: Automatico

**Codice campo modificato**

**Codice campo modificato**

1281 planktonic bacteria by image-analyzed epifluorescence microscopy, *Appl. Environ. Microbiol.*,  
 1282 49, 799–810, <https://doi.org/Schoffman, H., Lis, H., Shaked, Y., and Keren, N.: Iron-nutrient>  
 1283 interactions within phytoplankton, *Front. Plant Sci.*, 7, 1223,  
 1284 <https://doi.org/10.3389/fpls.2016.01223>, 2016.

1285 Sieracki, M. E., Johnson, P. W., and Sieburth, J. M.: Detection, enumeration, and sizing of  
 1286 planktonic bacteria by image-analyzed epifluorescence microscopy, *Appl. Environ. Microbiol.*,  
 1287 49, 799–810, <https://doi.org/10.1128/aem.49.4.799-810.1985>, 1985.

1288 Spiese, C. E., Kieber, D. J., Nomura, C. T., and Kiene, R. P.: Reduction of dimethylsulfoxide to  
 1289 dimethylsulfide by marine phytoplankton, *Limnol. Oceanogr.*, 54, 560–570, [https://doi.org/Spiese,](https://doi.org/Spiese, C. E., Kieber, D. J., Nomura, C. T., and Kiene, R. P.: Reduction of dimethylsulfoxide to)  
 1290 C. E., Kieber, D. J., Nomura, C. T., and Kiene, R. P.: Reduction of dimethylsulfoxide to  
 1291 dimethylsulfide by marine phytoplankton, *Limnol. Oceanogr.*, 54, 560–570,  
 1292 <https://doi.org/10.4319/lo.2009.54.2.0560>, 2009.

1293 Stefels, J.: Physiological aspects of the production and conversion of DMSP in marine algae and  
 1294 higher plants, *J. Sea Res.*, 43, 183–197, <https://doi.org/Stefels, J.: Physiological aspects of the>  
 1295 production and conversion of DMSP in marine algae and higher plants, *J. Sea Res.*, 43, 183–197,  
 1296 [https://doi.org/10.1016/s1385-1101\(00\)00030-7](https://doi.org/10.1016/s1385-1101(00)00030-7), 2000.

1297 Stefels, J., Steinke, M., Turner, S., Malin, G., and Belviso, S.: Environmental constraints on the  
 1298 production and removal of the climatically active gas dimethylsulphide (DMS) and implications  
 1299 for ecosystem modelling, *Biogeochemistry*, 83, 245–275, [https://doi.org/Stefels, J., Steinke, M.,](https://doi.org/Stefels, J., Steinke, M., Turner, S., Malin, G., and Belviso, S.: Environmental constraints on the)  
 1300 Turner, S., Malin, G., and Belviso, S.: Environmental constraints on the production and removal  
 1301 of the climatically active gas dimethylsulphide (DMS) and implications for ecosystem modelling,  
 1302 *Biogeochemistry*, 83, 245–275, <https://doi.org/10.1007/s10533-007-9091-5>, 2007.

1303 Stein, L. Y.: Methylamine: a vital nitrogen (and carbon) source for marine microbes, *Environ.*  
 1304 *Microbiol.*, 19, 2117–2118, [https://doi.org/Stein, L. Y.: Methylamine: a vital nitrogen \(and carbon\)](https://doi.org/Stein, L. Y.: Methylamine: a vital nitrogen (and carbon) source for marine microbes, Environ. Microbiol., 19, 2117–2118, https://doi.org/10.1111/1462-2920.13716)  
 1305 source for marine microbes, *Environ. Microbiol.*, 19, 2117–2118, [https://doi.org/10.1111/1462-](https://doi.org/10.1111/1462-2920.13716)  
 1306 2920.13716, 2017.

1307 Suleiman, M., Zecher, K., Yücel, O., Jagmann, N., and Philipp, B.: Interkingdom cross-feeding of  
 1308 ammonium from marine methylamine-degrading bacteria to the diatom *Phaeodactylum*  
 1309 *tricornutum*, *Appl. Environ. Microbiol.*, 82, 7113–7122, <https://doi.org/10.1128/aem.01642-16>,  
 1310 2016.

1311 Sun, J., Mausz, M. A., Chen, Y., and Giovannoni, S. J.: Microbial trimethylamine metabolism in  
 1312 marine environments, *Environ. Microbiol.*, 21, 513–520, [https://doi.org/Suleiman, M., Zecher, K.,](https://doi.org/Suleiman, M., Zecher, K., Yücel, O., Jagmann, N., and Philipp, B.: Interkingdom cross-feeding of ammonium from marine methylamine-degrading bacteria to the diatom Phaeodactylum tricornutum, Appl. Environ. Microbiol., 82, 7113–7122, https://doi.org/10.1128/aem.01642-16, 2016.)  
 1313 Yücel, O., Jagmann, N., and Philipp, B.: Interkingdom cross-feeding of ammonium from marine  
 1314 methylamine-degrading bacteria to the diatom *Phaeodactylum tricornutum*, *Appl. Environ.*  
 1315 *Microbiol.*, 82, 7113–7122, <https://doi.org/10.1128/aem.01642-16>, 2016.

1316 Sun, J., Mausz, M. A., Chen, Y., and Giovannoni, S. J.: Microbial trimethylamine metabolism in  
 1317 marine environments, *Environ. Microbiol.*, 21, 513–520, [https://doi.org/10.1111/1462-](https://doi.org/10.1111/1462-2920.14461)  
 1318 2920.14461, 2019.

1319 Suttle, C. A.: Viruses in the sea, *Nature*, 437, 356–361, <https://doi.org/Suttle, C. A.: Viruses in the>

Codice campo modificato

Codice campo modificato

Codice campo modificato

Codice campo modificato

Codice campo modificato

Codice campo modificato

1320 [sea, Nature, 437, 356–361, https://doi.org/10.1038/nature04160](https://doi.org/10.1038/nature04160), 2005.

1321 Taubert, M., Grob, C., Howat, A. M., Burns, O. J., Pratscher, J., Jehmlich, N., von Bergen, M.,  
 1322 Richnow, H. H., Chen, Y., and Murrell, J. C.: Methylamine as a nitrogen source for  
 1323 microorganisms from a coastal marine environment, *Environ. Microbiol.*, 19, 2246–2257,  
 1324 <https://doi.org/10.1111/1462-2920.13709>, 2017.

1325 Vaqué, D., Agustí, S., and Duarte, C. M.: Response of bacterial grazing rates to experimental  
 1326 manipulation of an Antarctic coastal nanoflagellate community, *Aquat. Microb. Ecol.*, 36, 41–52,  
 1327 <https://doi.org/10.3354/ame036041>, 2004.

1328 Ward, B. B. and Bronk, D. A.: Net nitrogen uptake and DON release in surface waters: importance  
 1329 of trophic interactions implied from size fractionation experiments, *Mar. Ecol. Prog. Ser.*, 219, 11–  
 1330 24, <https://doi.org/10.1002/cyto.990100519>, 1989.

1331 Ward, B. B. and Bronk, D. A.: Net nitrogen uptake and DON release in surface waters: importance  
 1332 of trophic interactions implied from size fractionation experiments, *Mar. Ecol. Prog. Ser.*, 219, 11–  
 1333 24, <https://doi.org/10.3354/meps219011>, 2001.

1334 Wheeler, P. A. and Hellebust, J. A.: Uptake and concentration of alkylamines by a marine diatom:  
 1335 effects of H<sup>+</sup> and K<sup>+</sup> and implications for the transport and accumulation of weak bases, *Plant*  
 1336 *physiology*, 67, 367–372, 1981.

1337 Wheeler, P. A. and Kirchman, D. L.: Utilization of inorganic and organic nitrogen by bacteria in  
 1338 marine systems I, *Limnology and Oceanography*, 31, 998–1009, 1986.

1339 Wheeler, P. A., North, B. B., and Stephens, G. C.: Amino acid uptake by marine phytoplankters  
 1340 1, 2, *Limnology and Oceanography*, 19, 249–259, 1974.

1341 Wheeler, P. A., North, B. B., and Stephens, G. C.: Amino acid uptake by marine phytoplankters  
 1342 1, 2, *Limnology and Oceanography*, 19, 249–259, 1974.

1343 Wickham, H.: ggplot2: Create Elegant Data Visualisations Using Grammar of Graphics,  
 1344 Comprehensive R Archive Network (CRAN), 2023.

Codice campo modificato

Codice campo modificato

ha formattato: Colore carattere: Automatico

Codice campo modificato

Codice campo modificato

Formattato: SpazioPrima: 12 pt, Interlinea: multipla  
 1.15 ri, Bordo: Superiore: (Nessun bordo), Inferiore:  
 (Nessun bordo), A sinistra: (Nessun bordo), A destra:  
 (Nessun bordo), Tra : (Nessun bordo)

1357 Wohl, C., Capelle, D., Jones, A., Sturges, W. T., Nightingale, P. D., Else, B. G. T., and Yang, M.:  
1358 Segmented flow coil equilibrator coupled to a proton-transfer-reaction mass spectrometer for  
1359 measurements of a broad range of volatile organic compounds in seawater, *Ocean Sci.*, 15, 925–  
1360 940, <https://doi.org/10.5194/os-15-925-2019>, 2019.

Codice campo modificato

1364 Wohl, C., Villamayor, J., Galí, M., Mahajan, A. S., Fernández, R. P., Cuevas, C. A., Bossolasco,  
1365 A., Li, Q., Kettle, A. J., Williams, T., Sarda-Esteve, R., Gros, V., Simó, R., and Saiz-Lopez, A.:  
1366 Marine emissions of methanethiol increase aerosol cooling in the Southern Ocean, *Sci. Adv.*, 10,  
1367 eadq2465, <https://doi.org/10.1126/sciadv.adq2465>, 2024.

Codice campo modificato

1371 Wu, M., McCain, J. S. P., Rowland, E., Middag, R., Sandgren, M., Allen, A. E., and Bertrand, E.  
1372 M.: Manganese and iron deficiency in Southern Ocean *Phaeocystis antarctica* populations  
1373 revealed through taxon-specific protein indicators, *Nat. Commun.*, 10, 3582, <https://doi.org/10.1038/s41467-019-11426-z>, 2019.

Codice campo modificato

1378 Yentsch, C. S. and Menzel, D. W.: A method for the determination of phytoplankton chlorophyll  
1379 and phaeophytin by fluorescence, *Deep Sea Res. Oceanogr. Abstr.*, 10, 221–231,  
1380 [https://doi.org/10.1016/0011-7471\(63\)90358-9](https://doi.org/10.1016/0011-7471(63)90358-9), 1963.

Codice campo modificato

1383 Zhang, Q., Jia, S., Chen, W., Mao, J., Yang, L., Krishnan, P., Sarkar, S., Shao, M., and Wang, X.:  
1384 Contribution of marine biological emissions to gaseous methylamines in the atmosphere: An  
1385 emission inventory based on multi-source data sets, *Sci. Total Environ.*, 898, 165285,  
1386 <https://doi.org/10.1016/j.scitotenv.2023.165285>, 2023.

Codice campo modificato

1390 Zu, H., Chu, B., Lu, Y., Liu, L., and Zhang, X.: Rapid iodine-oxoacid nucleation enhanced by  
1391 dimethylamine in broad marine regions, *Atmos. Chem. Phys.*, 24, 5823–5835, <https://doi.org/10.5194/acp-24-5823-2024>, 2024.